Book of Proceedings

Seventh Workshop

"Solar Influences on the Magnetosphere, Ionosphere and Atmosphere",

Sunny Beach, Bulgaria, 1-5 June 2015

Organized by:

Space Research and Technologies Institute

Bulgarian Academy of Sciences

Scientific Organizing Committee

Editors: **Katya Georgieva, Boian Kirov, Dimitar Danov**

CONTENT

CONTENT

Development of a Greek solar map based on solar model estimations*

Harry D. Kambezidis[1], *Basil E. Psiloglou*[1], *Kosmas A. Kavadias*[2], *Athanasios G. Paliatsos*[3], *Aristides Bartzokas*[4]

[1]Atmospheric Research Team, Institute of Environmental Research and Sustainable Development, National Observatory of Athens, Greece
[2]Laboratory of Soft Energy Applications & Environmental Protection, TEI of Piraeus, Greece
[3]Laboratory of Environmental Technology, Electronic Computer Systems Engineering Department, TEI of Piraeus, Greece
[4]Laboratory of Meteorology, Department of Physics, University of Ioannina, Greece
E-mail: harry@noa.gr

*Joint funding between KRIPIS-THESPIA and ARCHIMED programmes

ABSTRACT

The realization of Renewable Energy Sources (RES) for power generation as the only environmentally-friendly solution, moved solar systems to the forefront of the energy market in the last decade. The capacity of solar power doubles almost every two years in many European countries, including Greece. This rise has brought the need for reliable predictions of meteorological data that can easily be utilized for proper RES-site allocation. The absence of solar measurements has, therefore, raised the demand for deploying a suitable model in order to create solar maps. The generation of a solar map for Greece could provide solid foundations on the prediction of the energy production of a solar power plant installed in the country, by providing an estimation of the solar energy acquired at each longitude and latitude of the map. In the present work, the Meteorological Radiation Model (MRM), a broadband solar radiation model, is engaged. This model utilizes common meteorological data, such as air temperature, relative humidity, barometric pressure and sunshine duration, in order to calculate solar radiation for areas where such data are not available. Hourly values of the above meteorological parameters are used from 39 meteorological stations, evenly dispersed around Greece; hourly values of solar radiation are, therefore, calculated through MRM. Then, by using an integrated spatial interpolation method, a Greek solar energy map is generated, providing annual solar energy values all over Greece.

Keywords: MRM, Meteorological Radiation Model, solar radiation, Greek solar map

INTRODUCTION

Solar power systems have been at the forefront of the global energy market for at least one decade. In the meantime, the world realized that the only environmentally-friendly solution concerning power generation is the implementation of RES. In this context, following the rapid development of wind energy, solar power systems also presented remarkable market progress. At the same time, a rapid increase in installations of photovoltaic systems has been recorded in many European countries, including Greece, where during the recent period the installed photovoltaic capacity almost doubles every two years with total installations in 2013 exceeding 2.5 GW_e. It is, therefore, obvious that there is an increased interest in the possession of up-to-date and accurate solar radiation data that play prime role in energy-resource assessment of solar power systems.

In the recent years, solar radiation modelling utilizing existing climatic parameters, such as sunshine duration, cloud cover, relative humidity, air temperature etc., has shown remarkable progress. It is generally accepted that the use of models for solar radiation prediction, instead of using scattered ground-based measurements, is essential in solar energy systems design, because in most cases the low density and the limited number of solar

radiation measuring stations cannot describe the required variability of the climatic parameters involved (Muneer et al. 2007).

Several solar radiation models have appeared globally since the middle of the 20th century in order to generate solar radiation on horizontal plane, mostly under clear-sky conditions (e.g. Gueymard 2012). For example, the US National Solar Radiation Data Base provides hourly radiation data and Typical Meteorological Years (TMYs) for 239 US regions, with more than 90% of these having been derived from appropriate modelling (Maxwell 1998). Also, the European Solar Radiation Atlas (ESRA) is used for providing topography-based maps of solar irradiance in Europe and bordering countries (Page et al. 2001).

In the context of the above, a broadband model, which has been developed in Greece in the late 80's by the Atmospheric Research Team at the National Observatory of Athens for estimating solar radiation on horizontal surface, is the *Meteorological Radiation Model* (MRM). Since then, consecutive versions (the latest is version 5) of the model have been released with their full description given in a series of publications (Kambezidis et al. 1999, Psiloglou and Kambezidis 2007). Applications of MRM may be found in a variety of solar resource-assessment studies as well as in solar irradiance forecasting (Museruka and Mutabazi 2007, González et al. 2010). The main advantage of MRM is its simplicity in acquiring and using the necessary input data (i.e. four measured variables namely, air temperature, relative humidity, barometric pressure and sunshine duration).

Apart from the establishment of solar models, solar irradiance maps created by spatial interpolation of the estimated solar radiation by such models can provide a first insight of the solar potential at a candidate location. Several spatial interpolation methods can be found in the literature, such as natural neighbour interpolation (Dinis et al. 2009), inverse functions of distance (Pons and Ninyerola 2008), multiple linear regression (Daly et al. 1994), splines (McKenney et al. 2008) or kriging (Ruiz-Arias et al. 2011). The results of different studies, which compare deterministic and stochastic methods for the interpolation of environmental variables, show that the kriging method presents considerable advantages over the deterministic interpolation procedures (Luo et al. 2008). Such methods are based on the analysis of statistical properties, such as the data distribution and spatial correlation between the measured points among sites, providing reliable estimates for homogeneous terrains with similar climatic characteristics.

In the framework of the above, the present study utilizes geostatistics combined with model-estimated solar radiation data at several meteorological stations across the Greek territory by providing large-scale global solar radiation/energy. More precisely, the present work relies on collected synoptic data values from 39 meteorological stations belonging to the Hellenic National Meteorological Service (HNMS) during a 15-year period. The meteorological data include 3-hourly values of air temperature, relative humidity, barometric pressure and daily values of sunshine duration. By using linear interpolation on the 3-hourly values, an hourly database is generated. The corresponding database is amended with hourly values of global solar radiation on horizontal plane calculated by MRM. Finally, a solar map is developed by using spatial interpolated kriged data derived from solar radiation values at the 39 different locations across the country. A solar energy map so created aims to serve basic solar resource information and provide a general view of the distribution of solar radiation over the country.

METHODOLOGY

Fifteen (15) years of synoptic meteorological data were used, covering the period between 1985 and 1999. The measurements were obtained from 39 meteorological stations of the HNMS network evenly dispersed around Greece (see Figure 1).

Figure 1: Location of the 39 meteorological stations used in the study

The obtained meteorological data include 3-hourly values of air temperature, relative humidity and barometric pressure along with daily values of sunshine duration. It should be noted that the data underwent a further quality control through cleaning and gap-filling, in order to remove unwanted or false values and fill-in potentially corrupted or erroneous data points. More specifically, in order to detect and exclude erroneous data, a quality-control routine was applied, based on the physical range of the parameters and the maximum time-step variation (Psiloglou and Kambezidis 2007). By using linear interpolation on the 3-hourly values, an hourly database was generated.

The MRM model (version 5) was engaged, in order to generate solar radiation values for the 39 meteorological stations. According to the model, the direct-beam component of solar radiation normal to a horizontal plane at the earth's surface, under clear sky and natural atmosphere, is the extra-terrestrial radiation at the top of the atmosphere modified by absorption and scattering from its various constituents. Thus, during cloudless periods, the direct-beam radiation, I_b, received on a horizontal surface can be expressed as:

$$I_b = I_{ex} \cdot \cos\theta_z \cdot T_w \cdot T_r \cdot T_o \cdot T_{mg} \cdot T_a \quad (1)$$

where θ_z is the solar zenith angle, I_{ex} is the normal incidence extra-terrestrial solar radiation on the n_i-th day of the year; the T terms are the broadband transmittance functions for the absorption of water vapor (T_w), uniformly-mixed gases $(CO_2, CO, N_2O, CH_4 \text{ and } O_2)$ (T_{mg}), ozone (T_o), and total extinction (scattering and absorption by molecules and aerosols in the atmosphere)$(T_r, T_a, \text{respectively})$.

The diffuse sky radiation under clear-sky conditions is assumed to be made up of a portion of singly scattered by the atmospheric constituents (molecules and aerosol particles) direct beam radiation, I_{ds}, plus a multiple scattering component, I_{dm} (Psiloglou et al. 2000):

$$I_{ds} = I_{ex} \cdot \cos\theta_z \cdot T_w \cdot T_{mg} \cdot T_o \cdot T_{aa} \cdot 0.5 \cdot (1 - T_{as} \cdot T_r) \quad (2)$$

where T_{aa} is the aerosol transmittance function due to absorption only and T_{as} the aerosol transmittance due to scattering alone.

The total solar radiation received under clear-sky conditions on horizontal plane at the earth surface is the sum of the direct-beam and diffuse components, i.e.:

$$I_g = I_b + I_d \quad (3)$$

The corresponding direct-beam solar radiation under cloudy skies, I_{cb}, can be obtained by:

$$I_{cb} = I_b \cdot T_c \quad (4)$$

where T_c is the cloud transmittance.

Accordingly, the diffuse radiation at ground level under cloudy skies, I_{cd}, is the sum of the I_{cds} and I_{cdm} components. The singly-scattered portion of the diffuse radiation in the presence of clouds, I_{cds}, is computed by Barbaro et al. (1979):

$$I_{cds} = I_{ds} \cdot T_c + k^* \cdot (1 - T_c) \cdot (I_b + I_{ds}) \quad (5)$$

where k^* is an empirical transmission coefficient, whose value is a function of latitude and is obtained from Berland and Danilchenko (1961). The ground-reflected, atmospheric and cloud backscattered diffuse term, I_{cdm}, is modelled as in clear-sky conditions:

$$I_{cdm} = \frac{(I_{cb} + I_{cds})(a_g \cdot a_{cs})}{1 - a_g \cdot a_{cs}} \quad (6)$$

where a_g is the surface albedo and a_{cs} is the albedo of the cloudy sky.

Finally, the total solar radiation received under cloudy-sky conditions (partly or overcast) on horizontal surface is the sum of the horizontal direct-beam and diffuse components, i.e.:

$$I_{ct} = I_{cb} + I_{cd} \quad (7)$$

The obtained 15-year hourly solar database was used to develop a TMY for each of the 39 locations. A TMY is a dataset of hourly values of solar radiation and meteorological parameters composed of selected months from individual years, concatenated to form a complete year. A TMY represents the climatic conditions, typical over a long period at a location. For the generation of the 39 TMYs, the Sandia method was used (Hall et al. 1978) as modified by Pissimanis et al. (1988) and Argiriou et al. (1999). The Sandia method is an established empirical methodology for selecting individual months from different years over an available period, based on the Filkestein-Schafer (FS) statistics of 14 daily indices, namely maximum, minimum, mean and range of air temperature, relative humidity and barometric pressure and daily direct-beam and global solar energy. The weighted sum of FS statistics is calculated by using weighting factors for each daily index (Table 1).

Table 1: Weighting factors used for the FS statistics

Parameter	**Daily index**	**Weighting factor**
Air temperature	*Maximum*	3
	Minimum	3
	Mean	9
	Range	3
Relative humidity	*Maximum*	3
	Minimum	3
	Mean	9
	Range	3
Barometric pressure	*Maximum*	5
	Minimum	3
	Mean	3
	Range	3
Global radiation	*Daily sum*	25
Direct radiation	*Daily sum*	25
Sum		**100**

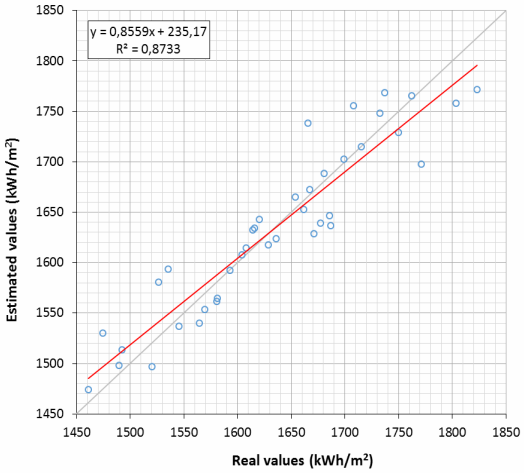

Figure 2: Comparison of estimated and real annual energy values for the 39 locations under investigation in Greece

and real values is very good as the coefficient of determination (R^2) exceeds 87%.

Based on the above methodology, an updated solar energy map was developed along with the corresponding predicted errors (Figure 3).

Figure 3 presents the global solar energy variation throughout the Greek region divided in 9 solar zones. The locations of the meteorological stations are coloured, based on their real annual solar energy value. According to the results, the annual solar energy in Greece ranges between 1450 and 1820 kWh/m^2, with southern areas possessing higher values of solar energy. The mean error of the estimated vs the real values is 1.94 kWh/m^2, which is relatively low.

The hourly solar radiation data of the 39 TMYs were used, in order to calculate the annual global solar energy obtained on horizontal plane. After testing several spatial interpolation methods, the Empirical Bayesian Kriging (EBK) was proved the most accurate for creating the Greek solar map. Fig. 2 presents a scatter plot of the estimated annual solar energy by EBK at the location of the 39 meteorological stations versus the real values as they were calculated by the TMYs. As indicated in the graph, the correlation between estimated

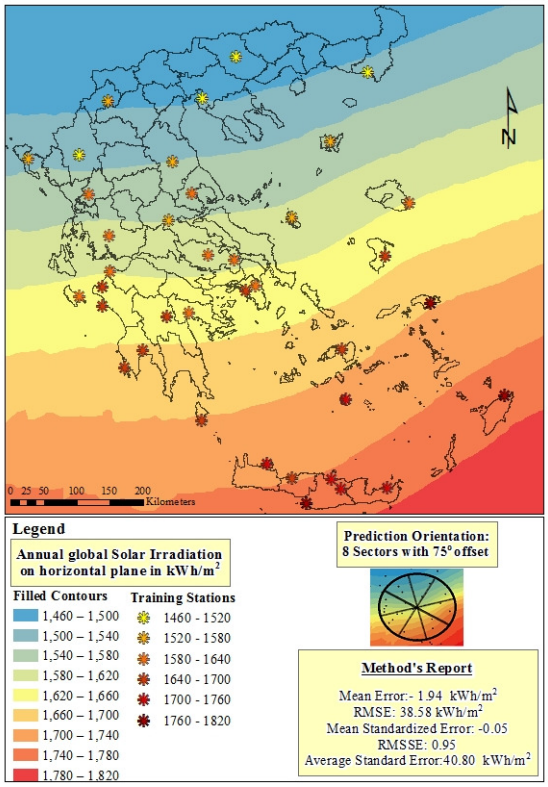

Fig. 3: Solar map of Greece based on the EBK method

CONCLUSIONS

The possession of up-to-date and accurate solar radiation data plays a key role in energy-resource assessment of solar power systems. Given the low density and limited number of solar radiation measuring stations, the use of solar radiation models is imperative. The present work presented an integrated procedure, which was used in order to develop an updated Greek solar map based on the solar radiation data estimated by the Meteorological Radiation Model at 39 meteorological stations belonging to the Hellenic National Meteorological Service network. The solar energy map so created provides solar resource information for any location over the country.

REFERENCES

Argiriou, A., Lykoudis, S., Kontoyiannidis, S., Balaras, C.A., Asimakopoulos, D.N., Petrakis, M. and Kassomenos, P., 1999, "Comparison of methodologies for TMY generation using 20 years data for Athens, Greece.", Solar Energy, Vol.66(1), pp.33–45.

Barbaro, S. B., Coppolino, S., Leone, C., and Sinagra, E., 1979, "An atmospheric model for computing direct and diffuse solar radiation", Sol. Energy, Vol.22, pp.225–228.

Berland, T. G. and Danilchenko, V. Y., 1961, "The continental distribution of solar radiation", Gidrometeoizdat, Leningrad.

Daly, C., Neilson, R.P. and Phillips, D.L., 1994, "A statistical-topographic model for mapping climatological precipitation over mountainous terrain", Applied Meteorology, Vol.33, pp.140–158.

Dinis, L.M., Jorge, R.M. and Belinha, J., 2009, "The natural neighbour radial point interpolation method: dynamic applications." Engineering Computations, Vol. 26, pp.911–949.

González, J., Serrano E. and Wiesenberg, R., 2010, "DNI forecasting using coupled WRF and MRM, enhanced with a neural network for CSP applications", Proc. Int. Conf. SolarPACES, Perpignan, France.

Gueymard, C.A., 2012, "Clear-sky irradiance predictions for solar resource mapping and large-scale applications: Improved validation methodology and detailed performance analysis of 18 broadband radiative models.", Solar Energy, Vol.86, pp.2145-2169.

Hall, I.J., Prairie, R.R., Anderson, H.E. and Boes, E.C., 1978, "Generation of a typical meteorological year", Annual Meeting of the American Section of the ISES.

Kambezidis, H.D., Adamopoulos, A.D. and Sakellariou, N.K., 1999, "The Meteorological Radiation Model", Int. Conf. ISES Solar World Congress, Jerusalem, Israel.

Luo, W., Taylor, M.C. and Parker, S.R., 2008, "A comparison of spatial interpolation methods to estimate continuous wind speed surfaces using irregularly distributed data from England and Wales", Climatology, Vol.28, pp.947–959.

Maxwell, E.L., 1998, "METSTAT – The solar radiation model used in the production of the National Solar Radiation Data Base (NSRDB)", Solar Energy, Vol.62, pp.263–279.

McKenney, D.W., Pelland, S., Poissant, Y., Morris, R., Hutchinson, M., Papadopol, P., Lawrence, K. and Campbell, K., 2008, "Spatial insolation models for photovoltaic energy in Canada", Solar Energy, Vol.82, pp.1049–1061.

Muneer, T, Younes, S. and Munawwar, S., 2007, "Discourses on solar radiation modelling", Renewable and Sustainable Energy Reviews, Vol.11, pp.551–602.

Museruka, C. and Mutabazi, A., 2007, "Assessment of global radiation over Rwanda." Proc. Int. Conf. on clean electrical power. Capri.

Page, J., Albuisson, M., and Wald L., 2001, "European solar radiation atlas: a valuable digital tool", Solar Energy, Vol.71, pp.81–83.

Pissimanis, D., Karras, G., Notaridou, V. and Gavra, K., 1988, "The generation of a 'typical meteorological year' for the city of Athens", Solar Energy, Vol.40(5), pp.405–411.

Pons, X. and Ninyerola, M., 2008, "Mapping a topographic global solar radiation model implemented in a GIS and refined with ground data", Climatology, Vol. 28, pp.1821–1834.

Psiloglou, B. E., Santamouris, M., and Asimakopoulos, D. N., 2000, "Atmospheric broadband model for computation of solar radiation at the Earth's surface. Application to Mediterranean climate", Pure Appl. Geophys., Vol.157, pp.829–860.

Psiloglou, B.E. and Kambezidis, H.D., 2007, "Performance of the meteorological radiation model during the solar eclipse of 29 March 2006", Atmospheric Chemistry and Physics, Vol.7, pp.6047–6059.

Ruiz-Arias, J.A., Pozo-Vazquez, D., Santos-Alamillos, F.J., Lara-Fanego, V. and Tovar-Pescador, J., 2011, "A topographic geostatistical approach for mapping monthly mean values of daily global solar radiation: A case study in southern Spain", Agricultural and Forest Meteorology, Vol.151, pp.1812-1822.

Cosmic Ray Intensity and Solar Activity Variations Possible Effects on the Rainfall in Turkey and Azerbaijan and Caspian Sea Level Changes

Famil Mustafa[1], *Ali Kilcik*[2], *Elchin Babayev*[1], *Atila Ozguc*[3]

[1] Shamakhy Astrophysical Observatory named after Nasiraddin Tusi, ANAS
[2] Department of Physics, Faculty of Science, Akdeniz University, Antalya, Turkey
[3] Kandilli Observatory and E.R.I., Bogazici University, Cengelkoy, Istanbul, Turkey
E-mail: famil_m@yahoo.com

ABSTRACT

The possible effects of cosmic ray intensity and solar activity variations on the rainfall over Turkey and Azerbaijan (middle-latitude Turkey - Caucasus/Caspian Sea region) and Caspian Sea level changes are investigated. Rainfall data for Turkey and Azerbaijan as climate parameter and sunspot number and cosmic ray intensity data as space weather indicators are used. Considered rainfall period was from January 1975 to the end of December 2008 meanwhile Caspian Sea level data were from 1900 to 2000. Multi-Taper Frequency Spectrum method (MTM) is applied to obtain the cyclic behavior of considered parameters. The most pronounced power peaks found by MTM were 1.2, 2.1-2.2 and 3.6-3.9 years (significance level > 99.9 %) which were reported earlier for some solar and cosmic ray activity indicators. Correlation analysis was also used in this study. Results did not reveal a remarkable correlation between rainfall and solar activity. It is concluded that in comparison to solar activity, cosmic rays have more significant effect on rainfall and sea level changes in studied regions and considered period. Cosmic ray intensity variations and solar wind changes caused effects could be considered as one of possible bridges in study of solar-climate relationships.

INTRODUCTION

Among the most debated questions in climate change are that of Sun-climate and cosmic ray-climate variability, which have attracted the attention of scientists for years (Kirkby, 2007; Dorman, 2009). Over the last years diverse reconstructions of past climate change have revealed some associations with cosmic ray variations recorded in cosmogenic isotope archives, providing persuasive evidence for solar or cosmic ray forcing of the climate. Sun-climate variability question is likely to remain open until a physical mechanism is established meanwhile observations suggest that cloud cover may be influenced by cosmic rays, which are modulated by the solar wind and, on longer time scales, by the geomagnetic field, so on.

Our recent study (Kilcik et al., 2008) shows that investigation of Sun–climate relationship on local scale may give better possibilities for understanding of the problem than global scale. The study of possible effects of cosmic ray intensity and solar activity variations on the rainfall over local regions could give interesting results.

The Caspian Sea is of exceptional interest to scientists because of its history of fluctuations in both area and depth, which offer clues to the complex geological and climatic evolution of the region. The Caspian Sea not only is an economical source but also a climatic regulator of the area. During many years there have been considerable fluctuations of the sea level.

One of the more fascinating aspects of the study of the Caspian Sea, however, is the study of long-term fluctuations over the decades and centuries gathered from archaeological, geographical, heliogeophysical and historical evidence. Long-term and seasonal fluctuations of the Caspian Sea level are considered to be mainly the result of fluctuations of components of its water balance. But possible role of space weather/climate influence through different mechanisms should not be neglected (i.e., Solov'eva in 2004 considered dependence of Caspian Sea level oscillations on the solar activity).

AIMS of STUDY

In this paper we made attempts to study possible effects of cosmic ray (CR) intensity and solar activity (SA) variations effects on the rainfall over two middle latitude located neighbor countries (Turkey and Azerbaijan) and Caspian Sea level changes. Long-period climate (precipitation and sea levels) data as well as relevant space weather parameters were used and modern mathematical methods were applied.

DATA AND METHODS

Rainfall data over Turkey and Azerbaijan are taken from Turkish State Meteorological Service, National Hydrometeorological Department of the Ministry of Ecology and Natural Resources of the Republic of Azerbaijan and NOAA's Satellite and Information Service (NESDIS), NNDC CDO. Monthly mean of rainfall cover 72 stations in Turkey. Azerbaijani rainfall data come from three main regions spread on latitude and longitude of this comparatively small country (Ganja, Lenkeran and Zagatala). Rainfall and cosmic ray data used in this study refer to the period 1975-2008. This study uses also Caspian Sea level changes data (1900-2000) taken from 5 stations around this largest inland sea. Sea level data were provided by the Institute of Geography, Azerbaijan National Academy of Sciences. The cosmic ray (CR) data is taken from the NOAA's National Geophysical Data Center (NGDC).

To remove monthly and seasonal changes, all griddled monthly data were smoothed with 12 month running average and anomalies of these smoothed data were calculated.

Following correlation and spectral analyses methods were applied in our study:

1. **Partial correlation analyses** (Pearson correlation method). We used yearly data from 1975 to 2008 for the "CR – Rainfall" correlations. This time period covers three solar cycles (21, 22 and 23). For the "CR – Caspian Sea level" correlations analysis we used only two cyclic data (1975 – 1997) due to lack of part of data for 23rd cycle. All cyclic correlations calculated for each cycle and data sets separately. The partial correlation analysis results are given in the Table 1.
2. **Spectral analysis** (period analysis). There has been used the Multi-Taper method (MTM) of spectral analysis, developed by Thomson (1982), to analyze periodical changes. This method reduces the variance of spectral estimates by using a set of tapers. In our study we used three sinusoidal tapers. For the period analyses monthly data sets were used. Our significance test is carried out with respect to red noise, since the rainfall and sea level records, have larger power at lower frequencies. All harmonic signals have been obtained by using of 90% confidence level.

RESULTS

In this study we have applied correlation and MTM spectral analysis methods to find (a) correlations between Turkey and Azerbaijan rainfall, Caspian Sea level changes and cosmic ray intensity variations; and (b) to build power spectrum which provides continuous temporal evolution of the entire range of periods.

Table 1. The partial correlation analyses results

	Cycle 21	Cycle 22	Cycle 23
CR - Azerbaijan rainfall	-0.47	-0.58	-0.46
CR -Turkey rainfall	-0.04	0.54	
CR – Caspian Sea Level	-0.50	0.17	

The correlation analyses results are given in Table 1. These are:

- Azerbaijani rainfall data show comparatively significant negative correlations with cosmic ray intensity data for all considered solar cycles;
- Turkey rainfall data show positive correlations only for solar cycle 22.
- Caspian Sea level data (when considering the period of 1975-2000) show comparatively significant negative correlation for solar cycle 21.

- Turkey and Azerbaijan rainfall data sets show different behaviors in respect to solar activity variations.

Correlation analysis of surface air temperature over Azerbaijan for cycles 21, 22 and 23 showed anti-correlation (-0.2, -0.08 and -0.42). It should be noted that correlation between Azerbaijani temperature and Caspian Sea level changes was 0.42 meanwhile "rainfall – sea level" correlation coefficient was – 0.73.

Power spectrum analysis reveals that:

- CR data show well-known periodicities such as 1.7, 2.2, 2.9, 1.1, 1.5, 10.7 years, etc., which are also revealed in solar activity variations;
- 1.2 years periodicity exists in all data sets used in this study (well seen in Azerbaijani rainfall and Caspian Sea level changes data with high CI);
- 3.7 years periodicity found in CR data also was revealed as in quasi forms in Turkey rainfall data (3.6 years) and Caspian Sea level changes data (3.9 years) meanwhile 2.2 years periodicity found in CR data also exists in both Azerbaijani (2.1 years) and Turkey rainfall data;
- 2.9 years periodicity found in CR data was revealed in all climate data.

DISCUSSIONS

Fig.1. shows that there is high level anti-correlation between CR and SSN. This well-known fact reveled also in our analyses, enables to consider CR intensity variations as one of possible bridges in Sun-climate relationship. Detailed analysis of Fig.1 shows that Azerbaijani and Turkey rainfall trends are not similar (not-coinciding) and there are even some periods (i.e., 1981-1983), when they show opposite trends. The time interval 1981-1983 corresponds to El Chichon volcanic activity (1981) period, and this interesting fact doubts that volcanic activity can have negative / positive effects on rainfall anomalies. In 1991 – 1995 there was another strong volcanic activity (Pinatubo) and both rainfall curves show a decreasing trend. The effects of these two big volcanic activities on incoming solar radiation are shown in Fig. 3.

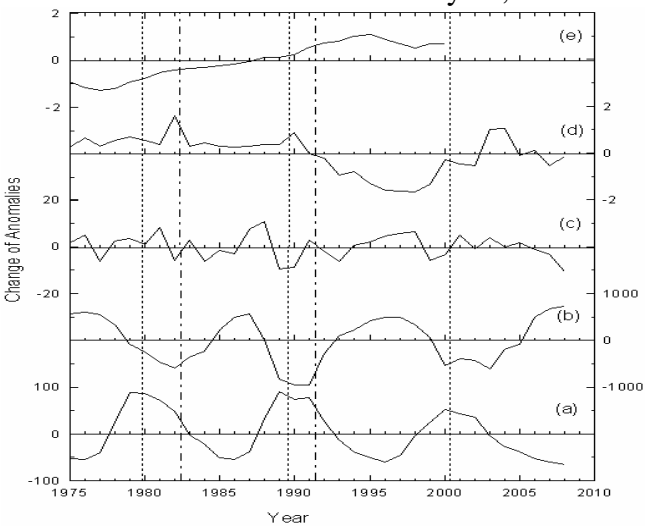

Fig.1. Changes of all data used in this study:
a) Sunspot number,
b) Cosmic ray intensity,
c) Rainfall over Turkey,
d) Rainfall over Azerbaijan,
e) Caspian

The other interesting period is 1991-2002; there is a strong deep in the Azerbaijani rainfall data for this period (our correlation analysis also indicates this fact). Comparison of climate and CR data and correlation analyses show different results which depend on climate data. These differences may arise from other factors, such as different absorbing aerosol concentrations in the atmosphere, pressure / altitude differences of the data stations, isolation of the regions etc.

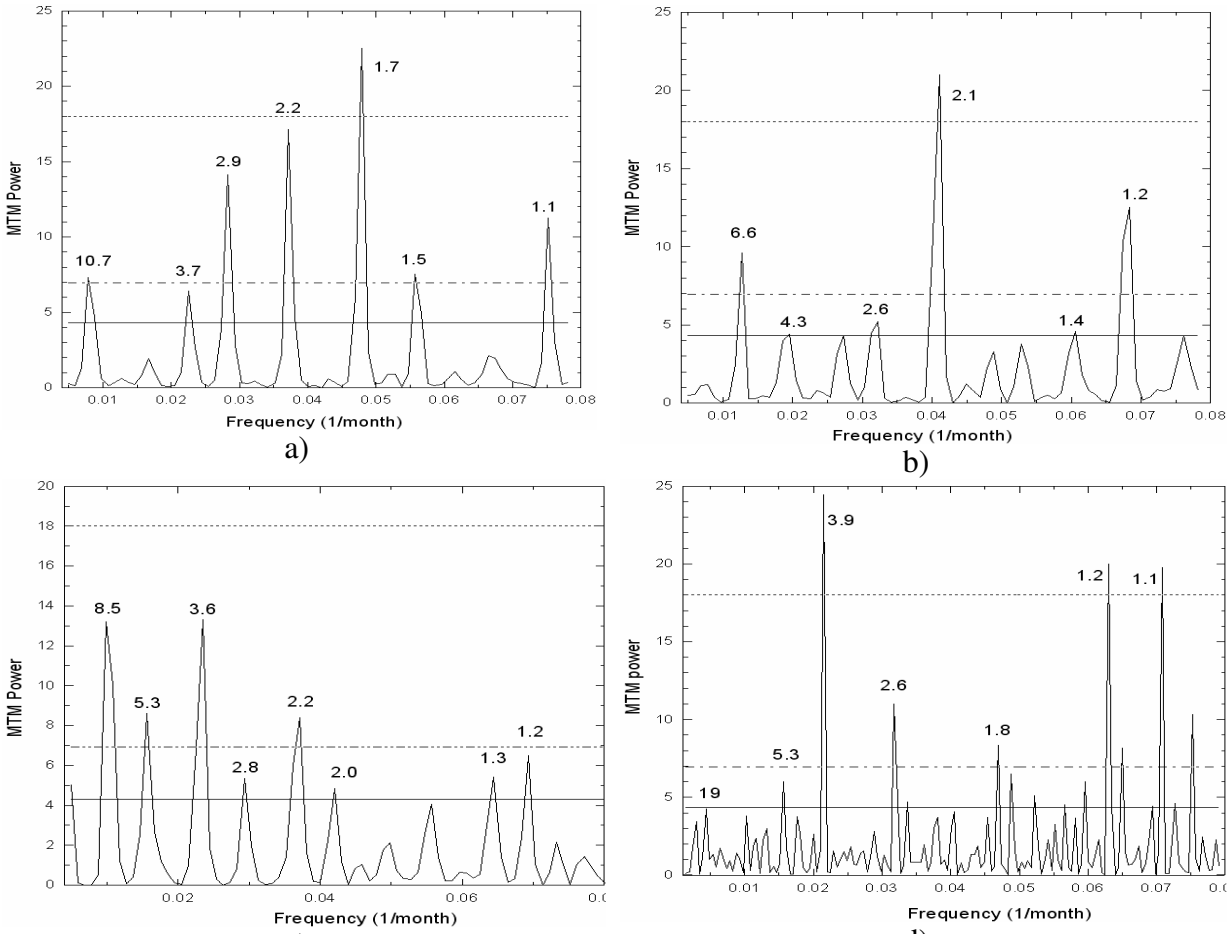

Fig.2. Power spectrums calculated for all considered data sets: a) CR, b) Rainfall of Turkey c) Rainfall of Azerbaijan, d) Caspian Sea level changes.

Kilcik (2005), Kilcik et al (2008) reported that the Sun – climate relation should be investigated on local scale due to these dependencies of Sun - climate system. As we already mentioned, periodicities found in our spectral analysis (see Fig. 2.) with high CI level, are displayed in many solar, geophysical phenomena, in IMF medium so on. Below we provide most interesting facts related to our study. The primary cause of the solar modulation of cosmic rays is not the level of sunspot activity, but the varying strength of the solar wind. 1.1, 1.3, 3.3, 5.5 year periods were found in the spectrum of solar wind velocity (1964-2003) (Nayar, 2006). The 1.3 year period is related to the variation in the rotation rate at the bottom of the solar convection zone (Howe et al., 2000). 1.1- and 2.4-year periods alongside with others were found in the power spectrum of sunspot numbers data during 1964 to 2003 meanwhile 5.5 year was seen in power spectrum of geomagnetic activity index Ap (Nayar, 2006). 3.9 year (very high CI) periodicity is quite close to the period 3.7-4 years, found either in geomagnetic activity or solar wind variations. A strong 1.3 year variation in solar wind speed occurs concurrently at different heliocentric distances around the ecliptic. The power in 1.3 year periods is found to follow the total number of sunspots and both vary approximately in phase. Krivova and Solanki (2002) found significant power at all multiplets of 1.3 year up to 10.4 year, which is nearly equal to the period of the solar cycle.

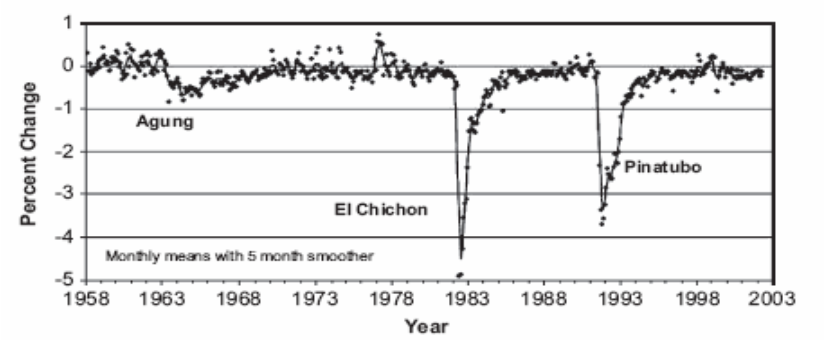

Fig.3. Net solar radiation measured at Mauna Loa Observatory, relative to 1958, showing the effects of major volcanic eruptions. Annual variations are due to the transport of Asian dust and air pollution to Hawaii. Figure is taken from Earth System Research Laboratory's web page (http:// www.esrl.noaa.gov/gmd/about/climate.html).

It should be noted that quasi-biennial oscillations (from ~1.5 to ~3.0 years) in various active events in the Sun are the second most powerful variation after the 11-year cycle (Ivanov et al, 2000).

CONCLUSIONS

Based on results of our preliminary study we conclude that:

- CR intensity variations can be considered as one of possible bridges in study of solar-climate relationships;
- There is an evidence that changes in CR intensity have effects on rainfall levels over Turkey and Azerbaijan as well as Caspian Sea level (latter could be due to rainfall effects on Volga river's flow level into the sea). Although this remains unclear yet, we also suggest that cloud cover may be influenced by cosmic rays, which are modulated by the solar wind and, on longer time scales, by the geomagnetic field and by the galactic environment of the Earth;
- Revealed in climate and sea level changes data periodicities (within 2-4 years interval) are well pronounced in solar wind and cosmic ray activity variations;
- We conclude that solar wind effects through different physical mechanisms (i.e., caused by high speed streams from coronal holes or fast CMEs-driven disturbances resulting in geomagnetic activity, Forbush decreases so on) could be considered one of major players in interpretation of results in space weather - climate relations' studies;
- Solar cycle 22 must be studied separately which generated a low number of flares in respect to its predecessor; correlation analyses show different (from other considered cycles 21 and 23, showing coinciding results) results namely for cycle 22;
- 1.2 year periodicity which is quite close to 1.3 year well-established periodicity seems to be one of important periods in solar-cosmic-ray-climate relationship;
- There was preliminarily found some correlation between sea level and total solar irradiance as well as were revealed (Fourier analysis) some signatures of Bruckner (~35 years) climatic cycle, but these questions must be studied in details and carefully;
- Mechanisms for the amplification of solar and cosmic ray forcing are not well established: despite the increasing evidence of its importance, "Sun - climate variability" link is likely to remain as open question; It is possible that solar activity variations during pre-industrial times were one of major causes of climate change. The Caspian Sea level changes (especially rising trend since 1978) may arise from the increase of greenhouse gases (GHG) concentration and/or oil pollution; Precipitation changes in the Volga River drainage basin also must be considered in analysis taking into account their possible forcing by solar activity and rainfall;

- Effect of volcanic activity on rainfall must be studied together with space weather influence;
- We should not focus only one single physical mechanism, i.e., space weather effects. There might be several possible physical mechanisms related to space weather changes that can operate together in determining the state and dynamics of climate on Earth. I.e., variations in ultraviolet and solar-induced changes in ozone (O3) may have a small effect on radiative forcing but additionally may affect climate through changing the distribution of solar heating and thus indirectly through a dynamical response;
- Further studies must be continued either on global or local scales taking into account all possible mechanisms (geographical, geological, ecological, heliogeophysical so on).

ACKNOWLEDGEMENTS

The CR data used in this study are taken from NGDC web page. We acknowledge the National Hydrometeorological Department of the Ministry of Ecology and Natural Resources of the Republic of Azerbaijan and NOAA Satellite and Information Service, NESDIS, NNDC CDO for rainfall data as well as Prof. Ramiz Mammadov (Azerbaijan) for the Caspian Sea level changes data.

REFERENCES

[1] Dorman L.I. The Role of Space Weather and Cosmic Ray Effects in Climate Change (Chapter 3). In: Climate Change: Observed Impacts on Planet Earth, ISBN: 978-0-444-3301-2, Trevor M. Letcher (ed.), Elsevier, 2009, pp.43-76.

[2] Howe R., J. Christensen-Dalsgaard, F. Hill, R. W. Komm, R. M. Larsen, J. Schou, M. J. Thompson and J. Toomre, "Dynamic variations at the base of the solar convection zone", Science, **287**, 456-460, 2000.

[3] Ivanov E.V., V.N. Obridko, and B.D. Shelting, Quasi-Biennial Oscillations of the Solar Magnetic Fields, Proc. 10th European Solar Physics Meeting", Solar Variability: From Core to Outer Frontiers", ESA **SP-506**, 847-850, 2000.

[4] Kilcik, A. Regional Sun–climate interaction. JASTP,**67**, 1573–1579. 2005

[5] Kilcik, A., Ozguc, A., Rozelot, J.P., and Yesilyurt, S., Possible traces of solar activity effect on the surface air temperature of Turkey, JASTP **70**, 1669–1677, 2008.

[6] Kirkby Jasper. Cosmic rays and climate. Surveys in Geophysics, **28**, 333-375, 2007

[7] Kirova N. A. and S. K. Solanki, "The 1.3-year and 156-day periodicities in sunspot data: Wavelet analysis suggests a common origin", A & A**, 394**, 701-706, 2002.

[8] Nayar Prabhakaran S.R. Periodicities in solar activity and their signature in the terrestrial environment. In: Proceedings of the ILWS Workshop, Goa, India: February 19-24, 2006, Edited by N. Gopalswamy and A. Bhattacharyya, "Solar Influence on the Heliosphere and Earth's Environment: Recent Progress and Prospects", 2006,170-177.

[9] Solov'eva N.N. Study of dependence of Caspian Sea level oscillations on the solar activity, S.-Petersburg, RGGMU Press, 2004, 70 pages (in Russian).

[10] Thomson, D.J., 1982. Spectrum estimation and harmonic analysis. IEEE Proceedings **70**, 1055–1096.

Estimation of Solar Activity Influence on Vertical Extent of Sprites

Peter Tonev

Space Research & Technology Institute, Bulgarian Academy of Sciences
E-mail: ptonev@bas.bg

Abstract.

Sprites in their lower portion (below 60 - 65 km) consist of downward propagating positive streamers which cause chemical disturbances (mainly of NO_x and O_3 constituents) in the lower mesosphere and upper stratosphere. A single sprite occupies thousands of cubic kilometers in the middle atmosphere. The total rate of sprites over the globe is estimated to be 1-3 per minute. The influence of 11-year solar activity (SA) variations on sprites' vertical extension, and thus, on their effects on chemical balance below 60 km is studied. For this goal, the altitude of termination of the sprite positive streamers is estimated as function of solar activity level by otherwise equal conditions. 11-year variations of this altitude can take place due to sensitivity of conductivity, and thus, of the sprite-driving electric fields, to SA. The streamer driving quasi-static electric fields below 60 km are evaluated by modeling during solar minimum and maximum, respectively by modeling based on the continuity equation for the Maxwell's current. The computations show that during solar minimum sprites due to +CG lightning of large charge moment change reach a lower altitude than during solar maximum; for weaker sprites the difference can be reversed, but smaller. The difference in lower sprite boundary determined by SA changes varies from several hundred meters to almost 1 km depending on the flash parameters and on conductivity in clouds.

Introduction

Red sprites are transient luminous events which occur in the height interval from 90 down to 40 km above nighttime thunderstorms. They are driven by quasi-static (QS) electric fields generated in this region typically after a positive cloud-ground (+CG) lightning discharge. Below ~65 km (in its mature portion) a sprite is essentially a net of positive streamers which propagate downwards with velocity in the range ~2×10^6 - ~2×10^7 m/s and are multiplied by branching. Sprites are widely studied as a factor of disturbances in chemical balance in strato-mesosphere (Arnone et al., 2008; Hiraki et al., 2008). The problems is considered about ability of sprites to be a link between solar activity (SA) and the chemical state of strato-mesosphere (at least, in specific regions on the Earth). Our arguments are: 1) In the sprite region from ~ 90 down to ~ 40 km, the factors for ionization and formation of conductivity are sensitive to the solar activity, hence, the post-lighting electric fields and sprite parameters can be also affected by SA; 2) A sprite consists of thousands of streamers which cause (especially below 60 km) chemical perturbations concerning NO_x and O_3 for hours and another small constituents (Hiraki et al., 2008; Arnone et al., 2008); 3) The global frequency of visible sprites estimated from satellite data is 1 - 3 per minute, and large part of sprites remain unobservable. In specific regions at middle geomagnetic latitudes where the GCR flux is the main ionization factor and the sprite activity is large (Great Plains in USA, South Africa, South America, etc.) sprites possibly disturb atmospheric chemistry balance permanently, and the 11-year variations of their chemical effects may be of importance.

If the vertical extent of sprites is controlled by the SA level, then significant 11-year changes in strato-mesospheric chemistry in these specific regions can take place during a solar cycle. Once created, the downward positive streamers of a sprite reach a termination height z_T which depends on the applied post-lightning QS electric field E so that:

$$E(z_T) = E_{cr+}(z_T), \qquad (1)$$

Here $E_{cr+}(z) = 4.4\times10^5 N(z)/N_0$ V/m is the threshold electric field of propagation of a positive streamer; N(z) is the density of neutral atmosphere at altitude z, $N_0 = N(z=0)$. Since the electric field $E(z)$ decreases with lowering of the altitude z of a streamer faster than E_{cr+}, Expr. (1) ensures support of streamer propagation at any height $z > z_T$ since $E(z) > E_{cr+}(z)$. We hypothesize that the streamer termination height z_T depends on SA changes since the streamer driving electric field E depends on conductivity σ, which is a function of SA as noted above.

The electric fields driving sprites

The distribution of the QS fields **E** generated by a +CG lightning discharge which produces a sprite depends on the flash parameters and on the night-time conductivity profile $\sigma(z)$. The distribution of the QS electric field **E** after a +CG lightning discharge is obtained by a 2D model (Tonev and Velinov, 2007) in cylindrical coordinates (r,φ,z) where z is the altitude and r is the radial distance from the charge removed by the flash. The continuity equation for the Maxwell's current is solved, $\nabla\cdot\mathbf{j}_M = 0$, where $\mathbf{j}_M = \mathbf{j}_C + \mathbf{j}_D$; $\mathbf{j}_C = \sigma\mathbf{E}$ and $\mathbf{j}_D = \varepsilon_0\partial\mathbf{E}/\partial t$ are the conduction and the displacement currents. The results obtained by Tonev and Velinov (2007) (their Fig.2) are for $E(z,t) = \mathbf{E}$ $(r=0, z, t)$ at sprite altitudes $40 \le z \le 90$ km. The conductivity is assumed to be not influenced by the electric field **E**. This is valid at altitudes considered (below 60 km) since the nighttime electron conductivity is negligible.

An important property of the electric field $E(z,t)$ at any altitude $z \le 60$ km where the relaxation time $\tau_R(z) = \varepsilon_0/\sigma(z)$ exceeds the lightning discharge time τ_L (typically τ_L is up to few milliseconds) is that the time peak $E_{peak}(z)$ reached by $E(z,t)$ persists approximately during the time interval $[\tau_L, \tau_R(z)]$. The inception time and velocity of the positive streamers of a sprite ensure that these streamers 'catch' the peak electric field E_{peak} at all altitudes below 60 km. Hence, the applied electric field at altitude z included in condition (1) is $E_{peak}(z)$.

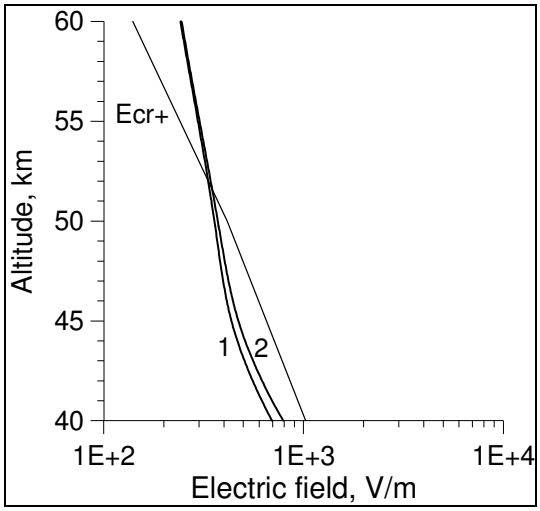

Figure. Peak QS electric field E_{peak} as function of altitude by maximum (curve 1) and minimum (2) solar activity generated by +CG lightning discharges from height 10 km by initial charge 100 C removed in time τ_L=1 ms. The thin line is for the threshold field E_{cr+} needed for propagation of a positive streamer.

The Figure shows the results for the height profiles of the peak QS electric field $E_{peak}(z)$ generated by the same parameters as in of the sprite-producing +CG lightning discharge and atmospheric conductivity profiles corresponding to solar minimum and solar maximum. Both profiles of E_{peak} are compared with the profile of E_{cr+}. The termination height z_T is obtained from condition (1) in each case. During solar minimum the termination height z_{Tmin} is by 0.4 km lower than that (z_{Tmax}) during solar maximum, due to change of E_{peak} by ~2%. This shows that even very small changes in E_{peak} (here they are due to SA change) can lead to significant

change of the termination height $\Delta z_T = z_{T\,max} - z_{T\,min}$, since the scale-heights of E_{cr+} and E_{peak} are close. The results obtained further are for a representative set comprising relevant intervals of variation of the parameters responsible for sprites.

Estimation of change of termination height

The change $\Delta z_T = z_{Tmax} - z_{Tmin}$ of termination height by transition from minimum to maximum SA by otherwise equal conditions (which concern the causative flash and conductivity) is obtained as follows:

$$\Delta z_T = \ln (C_E)\ H_E\ H_{Ecr} / (H_E - H_{Ecr}) \qquad (2)$$

Here H_E and H_{Ecr} are the scale-heights corresponding to the profiles of the electric fields $E_{peak}(z)$ and $E_{cr+}(z)$. H_{Ecr} is equal of the scale-height of N (between 40 and 60 km $H_{ecr} \sim -7.8$ km). H_E is represented by the expression $H_E(z) = [\ d \ln (E_{peak}(z) / \underline{dz})\ ]^{-1}$. $C_E(z)$ is the ratio between E_{peak} values at altitude z obtained by maximum and minimum SA, $C_E = E_{max}/E_{min}$ where E_{max} and E_{min} are the peak QS electric fields by maximum and by minimum SA. To determine C_E in Expr.(2), E_{peak} is estimated by different parameters of the causative +CG lightning discharge and conductivity profile. At an altitude z below 60 km the peak electric field E_{peak} does not depend on the actual lightning current waveform; it depends only on the initial charge Q_0 removed by lightning and on its altitude z_Q. We thus can assume that the charge decreases exponentially in time, $Q(t) = Q_0 \exp(-t/\tau_L)$. The 'profile' E_{peak} ($z \le 60$ km) is obtained as function of the lightning discharge parameters Q_0 and z_Q and of the average scale height h_σ of the conductivity between altitudes z_Q (height of the cloud charge Q_0) and z, $h_\sigma = (z - z_Q)/\ln[\sigma(z)/\sigma(z_Q)]$. Below ~60 km E_{peak} can be approximated in the form:

$$E_{peak} = Q_0\, P(\zeta_Q, \zeta_L, \zeta) / h_\sigma^2$$

where $\zeta = z/h_s$, $\zeta_Q = z_Q/h_s$, $\zeta_L = z_L/h_s$ are the dimensionless parameters. Below 60 km:

$$E_{peak}(\zeta_Q, \zeta) = Q_0\, C_R(z)\, P_0(\zeta_Q) \exp[z/(h_\sigma H_P)] / h_s^2 \qquad (3)$$

Here

$P_0(\zeta_Q) = 0.1547\zeta_Q^3 - 0.160\zeta_Q^2 + 2.345\zeta_Q$; $H_P(z_Q) = -0.04\zeta_Q^3 + 0.1022\zeta_Q^2 - 0.1065\zeta_Q + 2.272$

$C_R(z)$ is a correction coefficient which takes into account the influence of the conductivity profile and electric field below the height z_Q of the change:

$$C_R(z) = [R_e(0, z_Q)\, R(z_Q, Z_I)] / [R(0 < z < z_Q)\, R_e(z_Q < z < Z_U)],$$

$R[z_1, z_2]$ is the columnar electric resistance in the interval $[z_1, z_2]$ computed for the actual conductivity profile, and $R_e[z_1, z_2]$ is the one computed by exponential approximation of the same profile. It is derived from Expr.(3) that $H_E = h_\sigma H_P$. Typically, $h_\sigma \sim 4 - 6.5$ km, and $H_P \sim 3.4 - 3.6$ by absolute value, i.e. $|H_E| \sim 17 - 20$ km. It follows from (3) that the change of the SA level from SA minimum to maximum can lead to an increase or to decrease of the termination height depending on the sign of the difference $h_{\sigma max} H_{Pmax} - h_{\sigma min} H_{Pmin}$

Results and conclusions

For a representative estimation of z_T and $\Delta z_T = z_{max} - z_{min}$ due to transition from minimum to maximum SA eight cases are considered by varying the charge's altitude z_Q ($z_Q = 8$ km and 10 km), the total charge Q_0 removed by lightning ($Q_0 = 75$ C and 100 C), and the coefficient C_σ of reduction of conductivity in cloud ($C_\sigma = 0.2$ and 0.1, McGorman and Rust, 1998). The conductivity profiles $\sigma_{min}(z)$ and $\sigma_{max}(z)$ are obtained by respective modification of the basic profile $\sigma(z)$ obtained by measurements in a rocket experiment above a nighttime thunderstorm on Wallops Island (37.8°N, 75.5°W) at altitudes 18 - 70 km (Holzworth et al., 1985). The results for z_{min}, z_{max} and Δz_T for each case are given in the Table.

Table. Streamer termination heights z_{Tmax} and z_{Tmin}, and Δz_T by different model parameters

C_σ	z_Q, km	Q_0, C	z_{Tmax}, km	z_{Tmin}, km	Δz_T, km
0.2	8	75	56.1	56.3	–0.2
		100	49.5	49.6	–0.1
	10	75	51.8	51.5	0.3
		100	45.8	45.2	0.6
0.1	8	75	55.3	55.6	–0.3
		100	48.8	50.0	–0.2
	10	75	51.1	50.6	0.5
		100	45.0	44.2	0.8

In cases of higher located and larger charge Q_0 the streamers of a sprite reach lower altitudes by minimum solar activity (the vertical sprite extension is larger) than by maximum SA. The change of termination height Δz_T in considered cases reaches 0.8 km By the decrease of charge height and magnitude (by weaker sprites) the effect of variation of SA on the termination height diminishes and reverses its sign: during maximum SA the streamer termination height is slightly lower (few hundreds of meter) that that during minimum SA. The obtained results show that the suggested link between solar activity and the chemistry balance in lower mesosphere and upper stratosphere realized by sprites is not effective; a minor effect is possible only in regions at middle and higher geomagnetic altitudes, yet of large sprite activity.

References:

Arnone, E., A. Kero, et al. (2008), Seeking sprite-induced signatures in remotely sensed middle atmosphere NO2, *Geophys. Res. Lett.*, 35, L05807, doi:10.1029/2007GL031791.

Chen A.B., C.-L. Kuo, et al., (2008). Global distributions and occurrence rates of transient luminous events *J. Geophys. Res.*, 113, A08306, doi:10.1029/2008JA013101.

Hiraki, Y., Y. Kasai, H. Fukunishi, 2008. Chemistry of sprite discharges through ion-neutral reactions, *Atmos. Chem. Phys.*, 8, 3919–3928.

Holzworth, R.H., Kelley, M.C., et al. (1985). Electrical measurements in the atmosphere and the ionosphere over an active thunderstorm. 2.Direct current electric fields and conductivity. *J. Geophys. Res.*, **90**, 9824-9837 .

Li, J., and S. A. Cummer (2009), Measurement of sprite streamer acceleration and deceleration, *Geophys. Res. Lett.*, 36, L10812, doi:10.1029/2009GL037581.

Tonev P.T., P.I.Y. Velinov (2007). Atmosphere–ionosphere vertical electric coupling above thunderstorms of different intensity, *J. Atmos. Solar-Terr. Phys.*, **69**, 2007, 1203-1212.

MacGorman, D. R. and W. D. Rust, Electrical Structure of Thunderstorms, Oxford University Press, 1998, 432 p.

Coherent structures in the Es layer and neutral middle atmosphere

Zbyšek Mošna, Petra Koucka Knížová, Kateřina Potužníková

Department of Aeronomy, Institute of Atmospheric Physics, ASCR, Prague, Czech Republic
E-mail: zbn@ufa.cas.cz

Abstract.

The present paper shows results from the campaign performed during geomagnetically quiet period from June 1 to August 31, 2009. Within time-series of stratospheric and mesospheric temperatures at pressure levels 10 hPa to 0.1 hPa, mesospheric winds measured in Collm, Germany, and the sporadic E-layer parameters foEs and hEs measured at the Pruhonice station we detected specific coherent wave-bursts in planetary wave domain. Permanent wave-like activity is observed in all analyzed data sets. However, number of wave-like structures persistent in large range of height from the stratosphere to lower ionosphere is limited. The only coherent modes that are detected on consequent levels of the atmosphere are those corresponding to eigenmodes of planetary waves.

Introduction

Sporadic E layers (Es) are thin sheets of enhanced electron and metallic ion concentration located in the ionospheric E region. The critical frequency foEs (maximum plasma frequency of the layer) often exceeds the critical frequency of the E, or even F layer. The Es layer formation have been explained as a result of wind shear induced ionization transport (Whitehead, 1989; Axford, 1963). Vertical plasma drift leading to the ion convergence is controlled mainly by the zonal and meridional winds, when westward (northward) winds induce a downward, and eastward (southward) winds induce upward motion of the ions. The Es parameters foEs and hEs follow a regular daily pattern (Fig. 1) which is controlled mainly by wind shears in the lower thermosphere (Axford (1963); Whitehead (1989)). Further, they are driven by a longer-lasting neutral wave activity in the stratosphere and mesosphere. Review of Es behavior can be found in Haldoupis (2011).

Tidal and planetary waves

Mesosphere and Lower Thermosphere region (MLT) are significantly influenced by atmospheric waves. Well known and pronounced are diurnal solar tides and their harmonics (semidiurnal and terdiurnal tides). Planetary waves (PW) are large scale oscillations in the atmosphere usually with eigen-periods 2, 4, 5, 10, and 16 days (Forbes, 1995). They are responsible for a large part of energy transport between atmosphere regions in horizontal and vertical direction. They are forced in the troposphere by the topography, synoptic situation, or

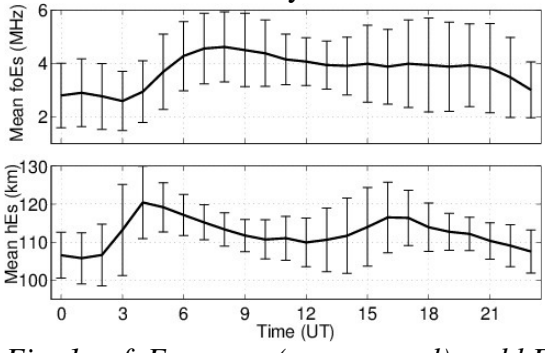

Fig. 1. – foEs means (upper panel) and hEs means (bottom panel) from summer 2009 measurement at Pruhonice. Vertical lines denote one standard deviation.

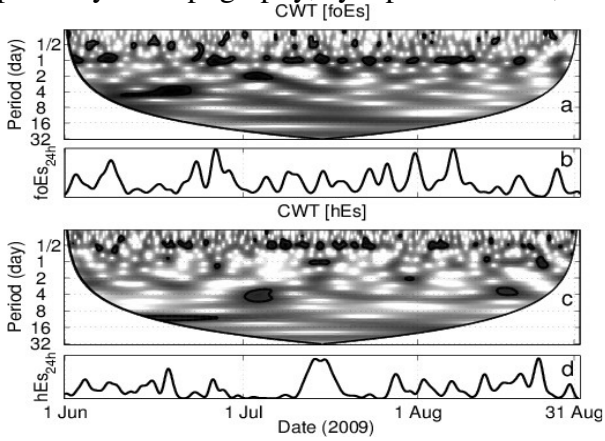

Fig. 2 - CWT of foEs (a) and hEs (c). Panels (b) and (d) show integrated power content at periods 23-25 h.

temperature differences between the sea and continents. Nonlinear efects in the terdiurnal tides excitation were proposed by (Jacobi and Fytterer, 2012). The amplitudes and vertical wavelengths of the terdiurnal tide depend strongly on season, latitude, and altitude. Arras et al. (2009) within GPS radio occultation data detected semidiurnal tidal response in the Es layer. Fytterer et al. (2014) used GPS observations and found that the migrating terdiurnal tides influence the Es formation at lower and midlatitudes at heights above 100 km. The effect of PW to the Es region was explained by acting of diurnal and semidiurnal tides modulated by the PW. Sauli and Bourdillon (2008) described tidal and planetary wave periodicity in the foEs and hEs (height of the Es layer) data. They attributed variability of diurnal mode to the Doppler-shift caused by 5 day planetary wave. Mosna and Koucka Knizova (2012) studied diurnal and planetary wave influence on the Es region represented by the foEs and hEs parameters. They found both coherent oscillations at diurnal period (and its harmonics) in the Es data and temperature data at the 10 hPa pressure level (approximately 30 km) at periods close to planetary eigen-periods by means of wavelet coherence.

Data and Method

We used critical frequencies foEs and heights hEs of the Es layers from June 1 to August 31, 2009. The ionospheric measurement was performed at the station Pruhonice (50°N, 15°E, LT = UT+1H) using the digisonde DPS-4. Es layer was almost permanently present. Time resolution of the measured and manually processed ionospheric data was 15 minutes, however we used 3h resolution for the analysis from time corresponding to wind and temperature data. The summer 2009 was generally of low geomagnetic activity. The neutral atmosphere data are represented by the temperature at pressure levels at 10 hPa, 5 hPa, 1 hPa, and 0.1 hPa corresponding roughly to 32 km, 37 km, 48 km, and 65 km, respectively. The temperatures are derived from the MERRA reanalysis for the grid point located at 50°N 15°E corresponding to the Pruhonice station and have 3 hour time resolution. The wind activity was described by means of prevailing meridional and zonal wind velocity (mean night velocity) measured at Collm, Germany (51.3°N, 13.0°E) using VHF meteor radar (Jacobi, 2012) at 82, 85, 88, 91, and 94 km. For description of wave activity in the data and detection of coherent structures we use methods of continuous wavelet transform and wavelet coherence applied in paper of (Mosna and Koucka Knizova (2012), Chapter 3. Method). Extension to the atmospheric applications can be found in (Torrence and Compo, 1998; Grinsted et al., 2004). To keep this paper consistent with the four above cited papers, we use the following acronyms CWT (Continuous Wavelet Transform) and WTC (Wavelet Transform Coherence). WTC shows how coherent the cross wavelet transform is in time period space. The wavelet coherence can be understood as localized correlation coefficient in time- frequency space. All plots showing CWT and WTC results are normalized to maximum value for all data or pairs of data (unitless representation).

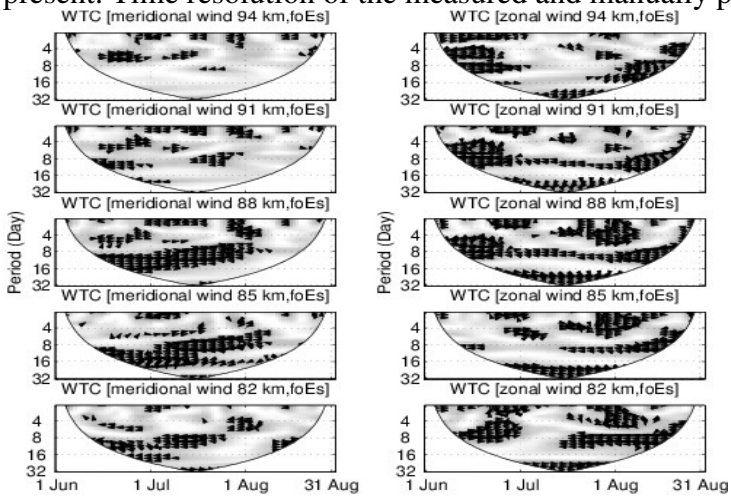

Fig. 3 - Wavelet coherence between meridional wind and foEs (left panels) and zonal wind and foEs (right panels) at different height levels.

Results and discussion

The sporadic E layers are controlled mostly by the diurnal tide which becomes dominant below 120 km, whereas the 12 h periodicity in Es is caused by the Descending Intermediate Layers (DILs) which are initiated by semidiurnal tides in the upper E region and move downward acting as parenting process for Es in the lower E region. Regarding shorter periods, published evidence about tide-like variations in sporadic E, e.g. 8 and 6 h periodicities, is rather limited (Haldoupis and Pancheva, 2006).

Continuous wavelet transform (CWT)

CWT of the sporadic E data reveals most dominant and stable periodicity at the tidal domain (Fig. 2). Pronounced terdiurnal, semidiurnal, and diurnal periods are present in both foEs and hEs data. The most prominent period in the foEs data is diurnal period, the most dominant period in the hEs data is the semidiurnal period. Further peaks are located at a wide band equal or above 2 days (2-3, 5, 10-16 days, Fig. 2 panels a and c). CWT of temperature data shows significant oscillations corresponding to the semidiurnal and diurnal domains. In temperature data at 0.1 hPa and 1 hPa, the semidiurnal period dominates over the diurnal period. Persistent wave-like domains are further located to the 2 day oscillation (0.1 hPa, 1 hPa, and 0.1 hPa), 3-4 day oscillation (10 hPa), 5 day oscillation (all temperature data) and 10 day oscillation (all temperature data, very strong for 1 and 5 hPa and with a prolonged period towards 16 days for 10 hPa). CWT of zonal and meridional wind data shows dominant periods at 2, 3-5, and 8 days. Zonal wind data show high power content at a band above 16 days and about 4-7 days peak in the middle of June at heights 88-94 km. Increased power in meridional winds at periods 8-10 days is present in the middle of July at heights 82-88 km.

Wavelet coherence (WTC)

WTC of temperature data and Es data intensifies at periods corresponding to semidiurnal, and diurnal waves. In planetary wave domain were detected oscillations at period 2 days and 5 days (all pairs of Es data and T except 10 hPa level). Bursts of common oscillations were localized at about 10 and 16 day period and wide bands of period above 16 days were present in WTC [T(0.1hPa),foEs] and WTC [T(1hPa,foEs)]. Wavelet coherence was further performed on both zonal and meridional wind data and Es parameters. 7-9 day periodicity was observed in all pairs wind vs. Es parameters. Meridional wind and foEs exhibit coherent 5 day periodicity for all height levels (Fig. 3, left panels). Meridional wind and hEs (not shown here) have coherent structures at 3-4 days and 7-8 days (heights 82 - 91 km). While some time-period domains vary with height levels of the neutral atmosphere data, there are several domains which are stable over whole or large vertical span. Coherent wave bursts can be found in all data pairs WTC [T,foEs] and WTC [T,hEs] at all pressure heights. Only those coherent structures which are present in at least three consequent height (pressure) levels are selected. These structures correspond to periods close to eigen modes of the PW. They seem to propagate upwards to the Es region where they influence/modify both height of the Es layer and maximum concentration of the Es layer.

Conclusion

We used stratosphere and mesosphere temperature data and mesosphere wind data as representatives of the neutral atmosphere, and critical frequency and height foEs and hEs representing ionospheric Es layer. Various areas of high coherence between neutral atmosphere and Es parameters exist in the whole studied vertical profile. However, only limited dominant periods detected in temperature and wind data coherent with the Es data were persistent along the vertical profile. Hence, we are able to detect them on several height (pressure) levels. These periods (2, 5, 9-10, and 15 day) correspond to the planetary eigen-modes. It confirms close relationship between planetary wave activity and sporadic E

properties and agrees with results proposed in Pancheva et al. (2003); Voiculescu et al. (2000); Mosna and Koucka Knizova (2012).

Acknowledgement: Authors acknowledge providing Collm meteor radar wind data by Prof. C. Jacobi of the Institute for Meteorology, University of Leipzig. This work was supported by Grant P210/12/2440, Grant of Ministry of Education, Youth and Sport (LG 13042) and Grant 16-24688S of the Grant Agency of the Czech Republic.

References

Arras, C., Jacobi, C., Wickert, J., 2009. Semidiurnal tidal signature in sporadic E occurrence rates derived from GPS radio occultation measurements at higher midlatitudes. In: Annales geophysicae. Vol. 27. Copernicus GmbH, pp. 2555-2563.

Axford, W. I., 1963. The formation and vertical movement of dense ionized layers in the ionosphere due to neutral wind shears. Journal of Geophysical Research 68 (3), 769-779.

Forbes, J. M., 1995. Tidal and planetary waves. The upper mesosphere and lower thermosphere: a review of experiment and theory, 67-87.

Fytterer, T., Arras, C., Homann, P., Jacobi, C., 2014. Global distribution of the migrating terdiurnal tide seen in sporadic e occurrence frequencies obtained from gps radio occultations. Earth, Planets and Space 66 (1), 1-9.

Grinsted, A., Moore, J. C., Jevrejeva, S., 2004. Application of the cross wavelet transform and wavelet coherence to geophysical time series. Nonlinear processes in geophysics 11 (5/6), 561-566.

Haldoupis, C., 2011. A tutorial review on sporadic E layers. In: Aeronomy of the Earth's Atmosphere and Ionosphere. Springer, pp. 381-394.

Haldoupis, C., Pancheva, D., 2002. Planetary waves and midlatitude sporadic E layers: Strong experimental evidence for a close relationship. Journal of Geophysical Research: Space Physics (1978-2012) 107 (A6), SIA-3.

Jacobi, C., 2012. 6 year mean prevailing winds and tides measured by vhfmeteor radar over collm (51.3n, 13.0e). Journal of Atmospheric and Solar-Terrestrial Physics 78, 8-18.

Jacobi, C., Fytterer, T., 2012. The 8-h tide in the mesosphere and lowerthermosphere over Collm (51.3N; 13.0E), 2004-2011. Advances in Radio Science 10 (22), 265-270.

Lastovicka, J., 2006. Forcing of the ionosphere by waves from below. Journal of Atmospheric and Solar-Terrestrial Physics 68 (3), 479-497.

Mosna, Z., Koucka Knizova, P., 2012. Analysis of wave-like oscillations in parameters of sporadic E layer and neutral atmosphere. Journal of Atmospheric and Solar-Terrestrial Physics 90, 172-178.

Pancheva, D., Haldoupis, C., Meek, C., Manson, A., Mitchell, N., 2003. Evidence of a role for modulated atmospheric tides in the dependence of sporadic E layers on planetary waves. Journal of Geophysical Research: Space Physics (1978-2012) 108 (A5).

Sauli, P., Bourdillon, A., 2008. Height and critical frequency variations s of the sporadic-E layer at midlatitudes. Journal of Atmospheric and Solar-Terrestrial Physics 70 (15), 1904-1910.

Torrence, C., Compo, G. P., 1998. A practical guide to wavelet analysis. Bulletin of the American Meteorological Society 79 (1), 61-78.

Voiculescu, M., Haldoupis, C., Pancheva, D., Ignat, M., Schlegel, K., Shalimov, S., 2000. More evidence for a planetary wave link with midlatitude E region coherent backscatter and sporadic E layers. In: Annales Geophysicae, 18, 1182-1196.

Whitehead, J., 1989. Recent work on mid-latitude and equatorial sporadic-E. Journal of Atmospheric and Terrestrial Physics 51 (5), 401-424.

Annual Tree Rings Widths and the "Sun-Climate" Relationship

Boris Komitov[1], *Peter Duchlev*[1], *Daniela Kirilova*[1], *Georgi Byandov*[2], *Nadya Kiskinova*[2]

[1]Institure of Astronomy and NAO - Rozhen, Bulgarian Academy of Sciences, Bulgaria,
[2]Astronomical Observatory "Yuri Gagarin", Stara Zagora, Bulgaria
E-mail: b_komitov@sz.inetg.bg

1. Introduction

The annual tree rings widths are ones of the good proxies for the climate changes as well as for the "Sun-climate" relationships and solar and geomagnetic activity in the past (Fritz et al., 1976; Rasspopov et al., 2008). The aim of this work is the presentation of results obtained from the measurements of annual rings widths of 44 tree samples, taken mainly from the mountain part of Bulgarian territory. There are 32 beech (Fagus), 11 oak (Quercus robur) and 4 pine (Pinus) samples (see Komitov et al., 2014a). The results in the light of the possible scenarios for solar activity and climate changes during the next few decades are discussed.

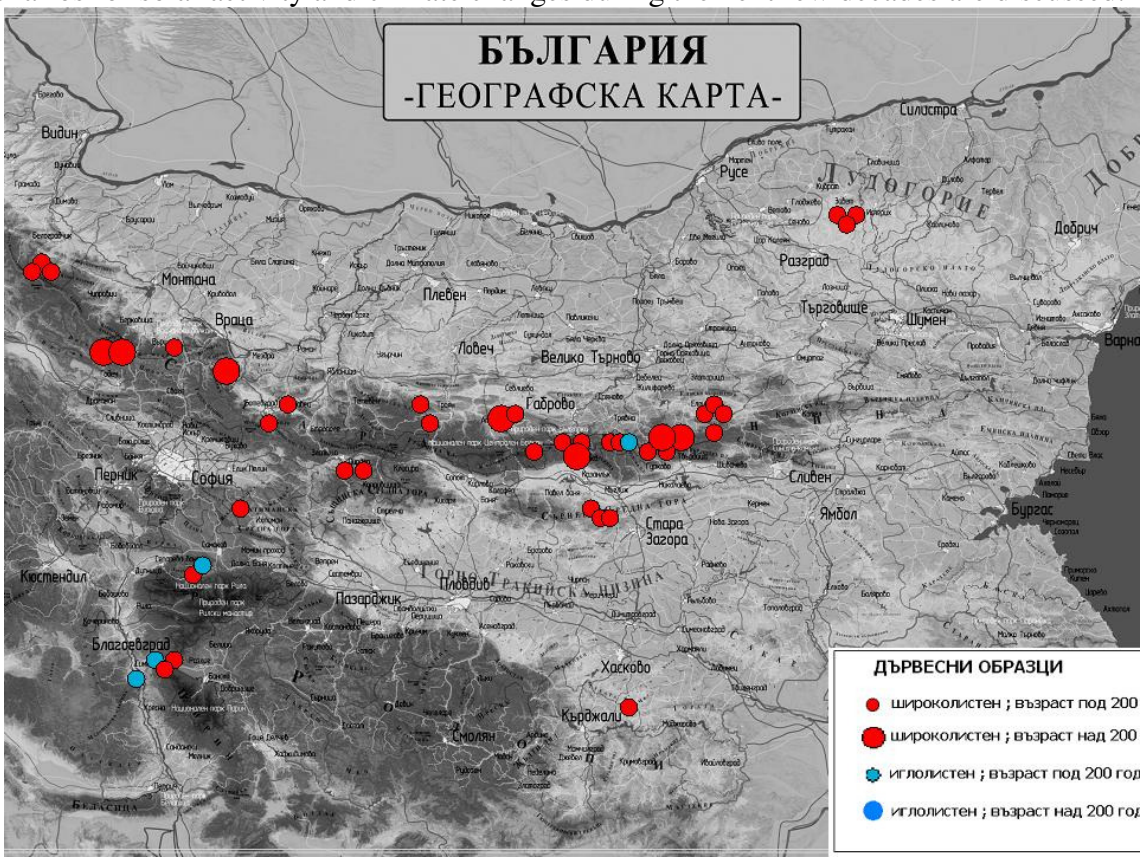

Fig. 1 The tree samples sites (red circles – beech and oak, blue circles - pine). The samples are signed by large circles.

2. Data and methods

From 1 to 8 radial profiles (depending on the quality of surface structure) of annual tree rings widths for each sample are measured. On this basis for each sample an averaged and smoothed by 5 years the radial profile (time series) has been obtained. These time series for existing in them of statistically significant trends and cycles has been investigated. The T-R periodogramm procedure for time series analysis (Komitov 1986, 1997) is used. On the basis of these results kinematical models of annual tree rings widths time series for the growth of two beech samples (Gurkovo-01 and Rositsa-01) were built. The latter are extrapolated for the next few decades. A climatic calibrations, based on instrumental data for rains and temperatures in near placed meteorological stations has been made for these time series.

That's why predictions about the possible climatic changes in Bulgaria into the warm season (May October) as well as for the solar and geomagnetic activity are possible. The full description of used methods and quantities is given in the study of Komitov et al. (2014b).

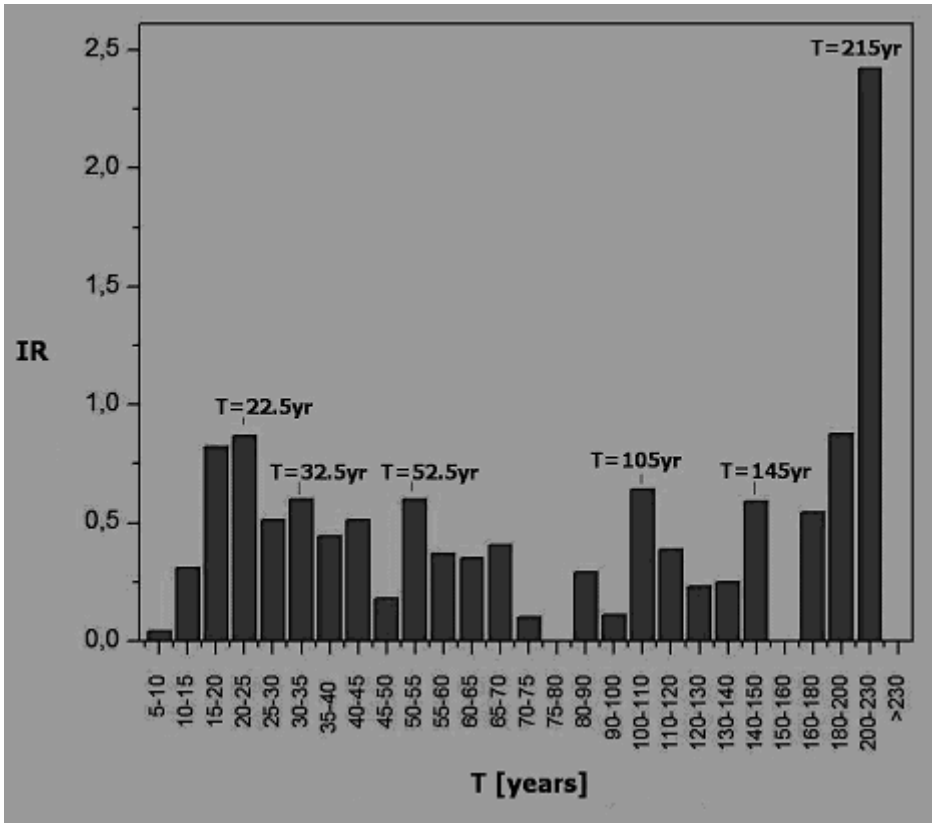

Fig. 2 The "index of expression" distribution (see Komitov et al, 2014a) IR for statistically significant cycles in the range 2 < T < 250 years

3. Results and analysis

A. On the base of the all 44 tree rings widths time series analysis it has been found that the best expressed oscillation in the sub centurial range is by length of ~ 22 years and also corresponds well to the solar magnetic 22yr (Hale) cycle. The above mentioned cycle is essentially better expressed if only the samples from South Eastern Bulgaria are taken into account.

B. There are also certain traces of cycles by length T of ~ 32.5, 52.5, 105, and 145 years.

C. For 6 of the all 7 oldest (age over 200 years) tree samples a presence of quasi sinusoidal trend –"hypercycle" with duration of $T \approx 215$ yr is detected too. The last one is in a good coincidence by phase with the solar 200-210 yr cycle, which is detected in almost all indirect ("historical") solar activity data series for "cosmogenic" isotopes (^{14}C and ^{10}Be), as well as in messages about aurora in Ancient and Middle Ages (Damon and Sonett, 1991; Dergachev and Chistyakov, 1993; Damon et al, 1997; Schove, 1955, 1983).

D. For the 7 all oldest (age over 200 years) samples a well – expressed minimum in annual rings width between 1795 and 1830 AD is also detected. It corresponds for generally dry summers during the start and end of so called solar "Dalton minimum". To our opinion traces of temporary increasing of tree rings widths in the course of sunspot cycle No 6 (1810 – 1823 AD) and near to the "Year without Summer" (1816 AD) are visible in different degree in all of these 7 longest time series.

E. The extrapolation of the annual rings width series kinematical model of our first tree sample (Gurkovo-01) (which was taken in 1983 AD) as an "epignosis" test has been used for the epoch after 1980 and up to 2012 AD. A continuous epoch of dry and warm

summers with short temporary breaking near to 2002-2005 AD has been predicted. As it is shown from the real instrumental meteorological data during the period 1980- 2013 AD the coincidence between this prediction and the real climate dynamics is very good.

F. The extrapolation of kinematical model for the sample Rositsa-01 about the epoch 2013 up to 2045 AD indicate for cooler and wet summers in Central North Bulgaria during the next tree decades. The corresponding tendencies should be very slow from 2013 to 2030 AD and with small 20-22 yr cycle contribution. It is an indication for weak solar cycles No 24 and 25. According to the model an essentially sharpen rainfall increasing should be expected after 2030 AD. It could be related to a very pecular structure of the pair solar cycles No 26 and 27.

REFERENCES

Damon, P. E. and Sonett, C. P., 1991, in *The Sun in Time*, eds.Sonett., C. P., Giampapa, M. S.

Damon, P., Periestykh, A., and Meese, D., 1997, 10Be/g:Production vs Accummulation in Recording the Schwabe and Hale Cycles, preprint (presented in 18th IAGA Assembly, Aug.1997, Uppsala)

Dergachev, V. A. and Chistyakov, V. F., 1993, *Izvestiya FTI*, 112. (in Russian)

Frittz, H., 1976, Tree Rings and Climate, Subsidiary of Harcourt Brace Jovanovich Publisher, London, New York, San Francisco.

Komitov, B., 1986, *Soln. Dannye Byull.* No 5, 73-78. (in Russian)

Komitov, B., 1997, *Bulg. Geophys. J.* 23, 74-82.

Komitov B., Duchlev, P., Kirilova, D., Bonev, T., Byandov, G., Kiskinova, N., Petrov, N., Nikolov, P., Tsvetkov Ts. and Stoycheva, A., 2014a, Catalog of tree samples, taken in 2013 AD in territory of Bulgaria , Alpha Visia, St. Zagora, Bulgaria. (in Bulgarian)

Komitov, B., Duchlev, P., Kirilova, D., Byandov, G. and Kiskinova, N., 2014b, The "Sun-Climate" connection and annual tree rings, Alpha Visia, St. Zagora, Bulgaria. (in Bulgarian)

Křivský, L. and Pejml, K.,1988, Solar activity, aurorae and climate in Central Europe in the last 1000 years, Bul.Astron. Inst. Chechosl. Acad. Sci., No75.

Rasspopov, O.M., Dergachev, V.A., Esper, J., Kozyreva, O., Frank, D., Ogurtsov, M., Kolstrom, T., Shao, X., 2008, *Palaeogeography, Palaeoclimatology, Palaeoecology* 259,16.

Schove, D. J., 1955, *J. Geophys. Res.* 60, 127.

Schove, D. J., 1983, *Sunspot Cycles* (Stroudsburg: Hutchinson Ross, Pennsylvania.)

Tropospheric systems influence on the ionospheric plasma

Koucká Knížová, P., Mošna, Z., Kouba, D., Potužníková, K., Boška, J.

Institute of Atmospheric Physics Czech Academy of Sciences, Prague, Czech Republic
E-mail: pkn@ufa.cas.cz

Abstract.

Correlation of long time series of the critical frequencies from European stations of vertical sounding is analysed with respect to latitudinal and longitudinal difference and surface distance of stations. Coefficients are high for raw data, subtracted mean courses but for fluctuations around mean as well. At the surface distance exceeding 1000km and/ or about 10 degrees of latitudinal difference between stations, the correlation coefficient of fluctuations decrease rapidly. As a possible source of the common influence on scale 1000km/10 degree we propose tropospheric systems that are known to be an important source of atmospheric waves in a broad period range. Large tropospheric mesoscale systems have typically up to 2000 km in diameter.

Introduction.

The most important factors that affect ionosphere are related solar and geomagnetic activity. However, the influence of the lower atmosphere through thermospheric chemistry and dynamics cannot be neglected. Within regions with collision dominated plasma (D and E regions) the influence is stronger than in the above laying regions F1 and F2.

Atmospheric waves propagating upward from the source region play an important role (see for instance Yigit and Medvedev, 2015). Their energy tends to be conserved and consequently the amplitude grows due to the decreasing atmospheric density. It has been proven experimentally that some atmospheric waves are able to penetrate up to the F2 layer height (Altadill et al., 2004; Boska and Sauli, 2001; Forbes and Leveroni, 1992; Forbes et al., 2000; Lastovicka and Sauli, 1999; Pancheva et al., 1994; Radicella et al., 2009; Sauli and Boska, 2001; among others).

Atmospheric waves.

Meteorological processes in the lower-lying layers, affect the ionosphere predominantly through the upward propagating waves and their modifications and modulations. Origin of the atmospheric waves is in periodic heating and cooling of the Earth atmosphere and surface and/or dynamics. Atmospheric waves propagate into the ionosphere mostly directly but the planetary waves can propagate upwards to the F region heights only indirectly, via various potential ways like modulation of the upward propagating tides. A review of the ionosphere forcing from lower laying atmosphere is provided by Lastovicka (2006). Troposphere is the most important region from where the atmospheric waves propagate upward. As the most important tropospheric sources of atmospheric waves especially gravity waves, topography, convection and wind shear (Fritts and Nastrom, 1992; Nastrom and Fritts, 1992) and jet stream (Fritts and Luo, 1992; Luo and Fritts, 1992) are identified.

Data.

For our analysis we use critical frequency (foF2) in the F2 around noon (mean value out of 10LT-14LT) from 15 European stations. These stations are following Arkhangels, Dourbes, Kaliningrad, Kiev, Lannion, Leningrad, Lycsele, Moscow, Paris, Poitiers, Pruhonice, Rome, Sodankyla, South Uist and Uppsala. Each time series cover at least one solar cycle, both periods of low and high solar activity

Method.

As in the paper Roux et al. (2012) time series of foF2 were split into long term and short term fluctuations and further analysed. The correlation coefficients were computed for all pairs of stations for original (raw) data, means, and fluctuations. Further, for all data the Continuous Wavelet Transform (CWT) and Wavelet Coherence (WTC) are computed. Detail description of wavelets can be found in Mallat (1998), Torrence and Compo (1998), Grinsted et al. (2004).

Results – Pearson correlation.

As in Roux et al. (2012) the correlation coefficients are high for all raw data, means and fluctuation derived from the foF2 series. Correlation coefficients of fluctuations are located into interval (0.2; 0.8). The highest correlation coefficients (close to 0.8) could be found only for latitudinal difference up to 5 degrees. For larger distances exceeding 5 degrees all the correlations decrease rapidly. In case of longitudinal dependency of the correlation coefficients, the highest values are up to the difference 10 degrees. Then the correlation coefficients decrease. The latitudinal decrease of correlation coefficient is faster than longitudinal. The same holds for correlations of raw data and trends.

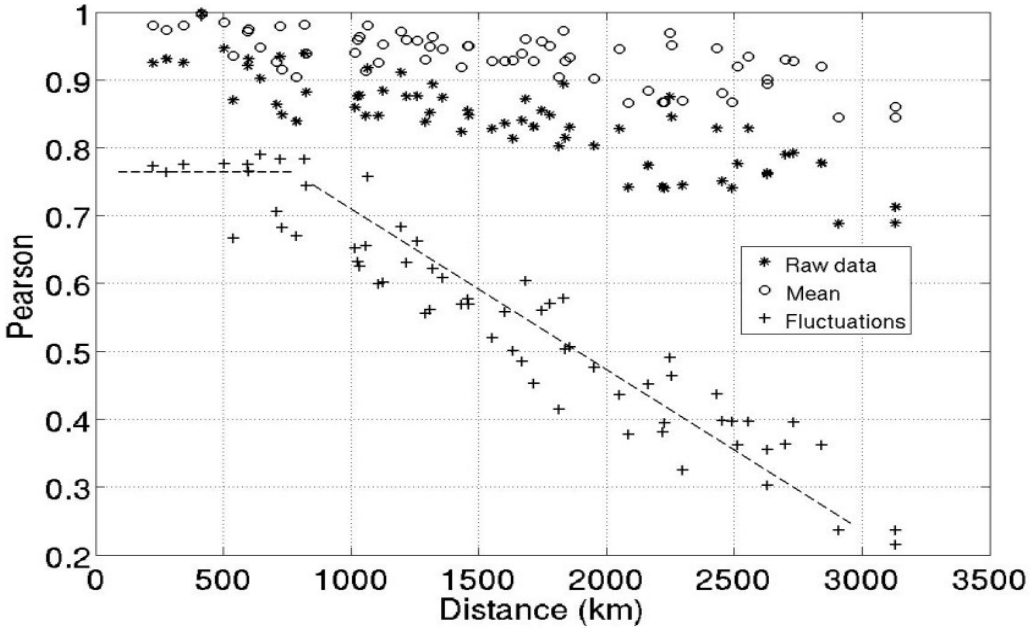

Figure 1. Correlation coefficient dependence on the surface distance.

On the plot of correlation coefficients with respect to actual surface (Fig.1.) the above described behaviour is even more significant. There is an evident change of the behaviour around distance 1000km. Supreme values (exceeding 0.7) of correlation are detected up to distance 1200 km. It holds for raw, mean and fluctuation correlations. Behaviour is best pronounced on fluctuations.

Results - Wavelet Transform Coherence.

Figure 2 shows an example of the WTC computed for pairs of stations Pruhonice-Rome (upper panel) and Pruhonice-Sodankyla (middle panel) on time scales between 4 and 64 days. Latitudinal differences of the stations are 7 degrees and 17 degrees, respectively. Surface distance of Pruhonice and Rome is 920 km, and Pruhonice and Sodankyla the distanceis 2050 km.

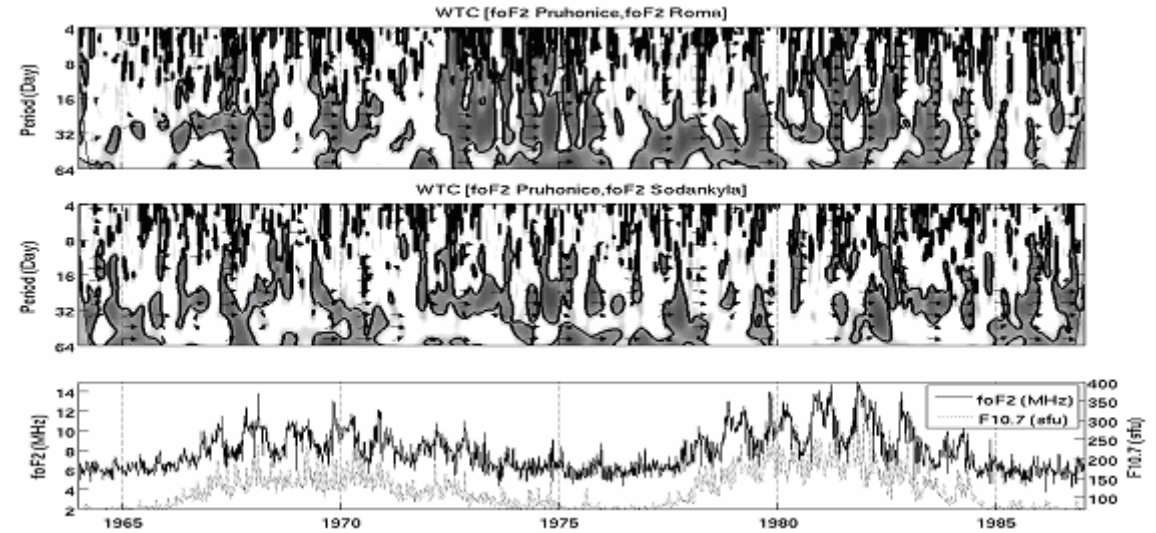

Figure 2. Wavelet Transform Coherence of time series of foF2 for pairs of stations Pruhonice-Rome and Pruhonice-Sodankyla.

On the bottom plot, foF2 from the Pruhonice and solar flux f10.7, are plotted together. On both WTC spectra there are areas of high common power. High WTC close to 27-day period is well seen on both spectra. WTC (Pruhonice, Rome) shows larger areas of coherency than WTC (Pruhonice, Sodankyla). WTC varies with the solar cycle. The largest areas of common coherent oscillations can be found on the descending phase of solar cycle (1973-1978).

Tropospheric mesoscale systems.

Lower atmospheric processes occur on wide range of spatial and temporal scales. The tropospheric phenomena are classified according to time and space scales in Orlanski (1975). Mesoscale processes represent motions of the order up to 2000 km on the horizontal scale and several days on the time scale. Hurricanes and frontal systems are representative phenomena of such processes.

Europe is influenced by various types of weather air-mass. The air circulation over Europe has a seasonal rhythm, which reflects the influence of the Arctic, polar and tropical air masses. It is dominated by western flow at the surface and also in the upper atmosphere. The cyclogenic processes strongly interact with significant orography, specifically the Alps and Pyrenees mountains (Kaspar and Muller, 2010). The most typical features of European weather is great variability (Bluestein, 1993; Hidore et al., 2009).

Conclusion.

On the plots of correlation coefficients we show an important change of behaviour at 1000 km surface and/or longitudinal distance 10 degrees. Up to the 1000 km surface and/or longitudinal distance 10 degrees the correlation coefficients are extremely high for raw, mean and even for fluctuations. Then they rapidly decrease. WTC of station pairs show areas of common high coherency within the analysed time range especially for periods of solar minima for time scales below 2 months. Higher power is found for closer pair of stations. The atmospheric waves of tropospheric and stratospheric origin may be responsible for this effect.

Acknowledgement: This paper has been supported by the Grant Agency of the Czech Republic (15-24688S) and Ministry of Education, Youth and Sports (LG13042).

References

Altadill, D., Apostolov, E.M., Boska, J., et al. Lastovicka, J., Sauli, P., 2004. Planetary and gravity wave signatures in the F-region ionosphere with impact on radio propagation predictions and variability. Ann Geophys, 47, 2-3, S, 1109-1119.

Bluestein, H. B., 1993. Synoptic-Dynamic Meteorology in Midlatitudes: Volume II: Observations and Theory of Weather Systems. ISBN-13: 978-0195062687 ISBN-10: 019506268X

Boska, J., Sauli, P., 2001. Observations of gravity waves of meteorological origin in the F-region ionosphere. Phys. Chem. Earth, 26 , 6, 425-428.

Forbes, J.M., Palo, S.E., Zhang, X., 2000. Variability of the ionosphere. JASTP, 62, 685–693.

Forbes, J.M., and Leveroni, S., 1992. Quasi 16-day oscillation in the ionosphere. GRL, 19, 10, 981-984.

Fritts, D. C., and Luo, Z., 1992. Gravity wave excitation by geostrophic adjustment of the jet stream. Part I: Two-dimensional forcing. JAS, 49, 861-697.

Fritts, D.C., and Nastrom, G.D. ,1992. Sources of mesoscale variability of gravity waves, II, Frontal, Convective and Jet stream excitation, JAS, 49, 111-127.

Grinsted, A., Moore, J. C., Jevrejeva, S., 2004. Application of the cross wavelet transform and wavelet coherence to geophysical time series. NPG, 11, 561–566. http://www.glaciology.net/

Hidore, J. J., Oliver, J.E., Snow, M., Snow, R., 2009. Climatology: An Atmospheric Science (3rd Edition), ISBN-13: 978-0321602053 ISBN-10: 0321602056

Kaspar, M., Müller, M., 2010. Variants of synoptic-scale patterns inducing heavy rains in the Czech Republic. Phys. Chem. Earth 35, 477–483.

Lastovicka, J., 2006. Forcing of the ionosphere by waves from below. JASTP, 68, 3–5, 479-497.

Lastovicka, J., and Sauli, P., 1999. Are planetary wave type oscillations in the F2 region caused by planetary wave modulation of upward propagating tides? ASR, 24, I I, 1473-1476.

Luo, Z., and Fritts, D. C., 1992. Gravity wave excitation by geostrophic adjustment of the jet stream. Part II: Three-dimensional forcing. JAS, 50, 1, 104-115.

Mallat, S., 1998. A Wavelet Tour of Signal Processing. Academic Press, San Diego.

Nastrom, G.D., Fritts, D.C., 1992. Sources of mesoscale variability of gravity-waves. 1. Topographic excitation. JAS, 49, 2, 101-110.

Orlanski, I., 1975. A Rational Subdivision of Scales for Atmospheric Processes. BAMS, 56, 5, 527-530.

Pancheva, D., Alberca, L.F. , de la Morena, B.A., 1994. Simultaneous observation of the quasi-two day variations in the lower and upper ionosphere. JASTP, 56, 43–50.

Radicella, S.M., Sauli, P., Jakowski, N., Kouba, D, Portillo, A., Herraiz, M., Strangeways, H.J., Zernov, N., Gherm, V., 2009. Space Plasma Effects. Ann Geophys, 52, 3-4, 359-372.

Roux, S.G., Koucká Knížová, P., Mošna, Z., Abry, P., 2012. Ionosphere fluctuations and global indices: A scale dependent wavelet-based cross-correlation analysis. JASTP, 90-91, 186-197. DOI: 10.1016/j.jastp.2012.03.014

Sauli, P., Boska, J. 2001. Tropospheric events and possible related gravity wave activity effects on the ionosphere. JASTP, 63, 9, 945-950.

Torrence, C. and Compo, G. P., 1998. A practical guide to wavelet analysis, BAMS, 79, 61–78, http://paos.colorado.edu/research/wavelets/

Yiğit, E., and Medvedev, A. S., 2015. Internal wave coupling processes in Earth's atmosphere, ASR, 55, 983–1003, doi:10.1016/j.asr.2014.11.020.

The Atlantic multidecadal oscillation influence on temperatures and on structural changes

R. Werner[1], *D. Valev*[1], *D. Danov*[1], *V. Guineva*[1] *and A. Kirillov*[2]

[1] Space Research and Technology Institute (SRTI), BAS,
Stara Zagora Department, Stara Zagora, Bulgaria
[2] Polar Geophysical Institute (PGI), Apatity, Russia
E-mail: rolwer52@yahoo.co.uk

Abstract.

The cooling and the following warming periods in the Northern Hemisphere are very well captured by the statistic models taking in consideration the Atlantic multidecadal oscillation (AMO). It is found that the AMO temperature influence increases from South to North, which is related to the heat transfer from the tropics to the Northern Atlantic by the thermohaline circulation. It is demonstrated, that structural breaks of the Northern Hemisphere and global temperatures are connected with AMO. The AMO influence removed temperature series show only one significant break. The strong AMO influence on the Northern Hemisphere and global temperatures will reduce the temperature increase in the next decades but when the AMO index will begin rising again the warming rates will achieve values close to the obtained ones during the last decades or greater than them due to higher dioxide content.

1. Introduction

AMO represents changes of the Sea surface temperatures variability in the North Atlantic with periodicities of roughly 70 years (Enfield**,** 2010)**.** AMO shows significant climate impacts, as correlations with rainfalls over continental parts of USA (Enfield, 2001), over Sahel (Folland et al., 1986) and North-East Brasil (Folland et al., 2001). Relations to North American and European climate (Sutton and Hudson, 2005) and connection with river flows (Enfield, 2001) were found. Some studies have proved an AMO contribution to higher frequency of Atlantic hurricanes and their energy (Goldberg et al., 2001, Wang and Dong, 2010). A link with the variability of the termohaline circulation was demonstrated (Delworth and Mann, 2000).

In this paper temperature anomalies of the three most important climate centers: the Goddard Institute for Space Studies (GISS) at NASA, the National Climatic Data Center (NCDC) at NOAA, both of USA, and the Hadley Centre at the Met Office of UK which collaborates with the Climate Research, are analysed.

2. Regression analysis methods

By means of a simple multiple regression of the global and hemisphere combined land/ocean, land and ocean surface temperatures against the carbon dioxide (CO_2) (Hansen et al.,2004), AMO (Enfield et al., 2001), the Pacific decadal oscillation (PDO) (Zhang et al., 1997 and Mantua et al., 1997), the Total Solar Irradiance (TSI) (Wang, Lean and Sheeley, 2005), the Southern oscillation (SO) (Trenberth, 1984), and Atmospheric Optical Depth (AOD) (Sato, 1993) the annual surface temperatures were modeled (without feedbacks). Because of the saturation effect of the absorption by CO_2 a logarithmic relation of CO_2 was used and the mixing ratio was related to the pre-industrial CO_2 level of 280 ppmv. Structure changes in the temperature time series are studied based on piecewise regression model (Seidel and Lazante, 2004). The regression analyses were performed stepwise with backward elimination of the most non-significant term at every step and the model coefficients were tested at a significance level of 0.95, where the autocorrelation of the residuals was taken into account (Werner et a., 2015).

2.1. Combined land-ocean Global and hemispheric temperature analysis

By the regression the CO_2 concentration is obtained as the most significant impact factor on the temperatures, as a whole the regression coefficient is approximately 3.0 and doesn't show hemispheric dependencies.

The increase of CO_2 produced a warming of 0.75ºC during the period 1900-2011 and it is not appreciably influenced by the hemispheric land-ocean distribution differences. In contrast the influence of AMO, which is the second important factor, has significantly greater regression coefficients in the Northern Hemisphere (NH). The mean AMO amplitude in NH is of the order of 0.13ºC for all three used data sets. For the Southern Hemisphere (SH) an mean influence of 0.03ºC is found only for the GISS data. The SO temperature influences do not exceed an absolute value of about 0.1ºC. Weak temperature impacts are obtained for TSI. Significant influences are obtained only for the GISS and NCDC data sets from SH, where the temperature response is smaller than 0.15ºC, and the temperature response from solar maximum to solar minimum is not greater than 0.12ºC. It is very important to stress, that the multiple correlation coefficients obtained here for all models are very high. The lowest values but higher than 0.92 are obtained for the SH models where the AMO influence is low or not significant. However, the explained variance is also higher than 0.85. The best correlation of 0.965 corresponding to 93% explained temperature variance is found for GISS and NCDC global temperature anomalies model. For the HadCrut3 data the corresponding values are 0.954 and 91%, respectively.

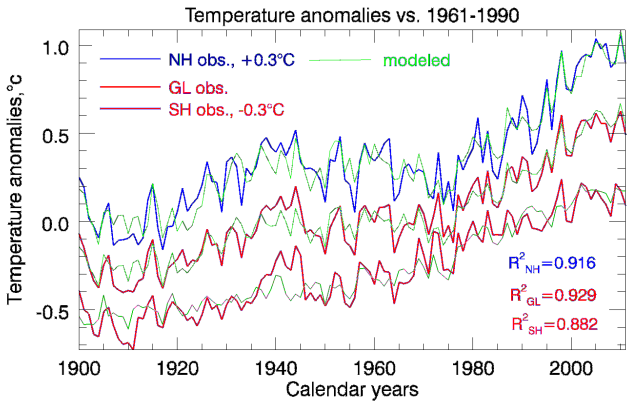

Fig.1. Observed global and hemisphere temperature anomalies by NCDC and the results of the modeled by regression temperature evolutions.

2.2. Analysis of the global temperatures separately over land and ocean

The obtained regression coefficients of the three used data sets do not show significant differences. The obtained CO_2 influences on the temperature anomalies over land are significantly greater, approximately two times, than the ones over the ocean by reason of feedback mechanisms. The increase of CO_2 produced a warming of approximately 0.6ºC and 1.2ºC over the oceans and the land, correspondingly, during the studied time period. For the AMO, SO and AOD influences no land/ocean differences are obvious.

2.3. Temperature forecast

AMO and the logarithmic term of CO_2 in the regression equations are the only long time terms. Our prognosis is based on a growth rate of 1.68 ppmv/year for CO_2, resulting from the linear regression for the last 30 years (1982-2011) and on the description of AMO by harmonic regression of first order with a period of 64 years and an amplitude of 0.208. Inserting the regression coefficients of the full regression model also for the expected values for the CO_2 content and the AMO index the prognosis ensemble mean temperatures are obtained for the forecast period 2012-2100.

Fig.2 presents the forecasts for the temperature evolution over land and ocean separately and for the combined land/ocean temperature obtained on the base of NCDC data set. The temperature over land from 1900 up to the end of our century will change approximately with 2.5°C. In contrast over the sea the temperature change will be only about 1.2°C, if the CO_2 concentration is going to increase with the same rate as it was observed in the last 30 years and if AMO is stable. In the next decades the warming rates will be smaller than the observed ones in the last 30 years due to the AMO influence, which will give us a chance to reduce the CO_2 emission in time.

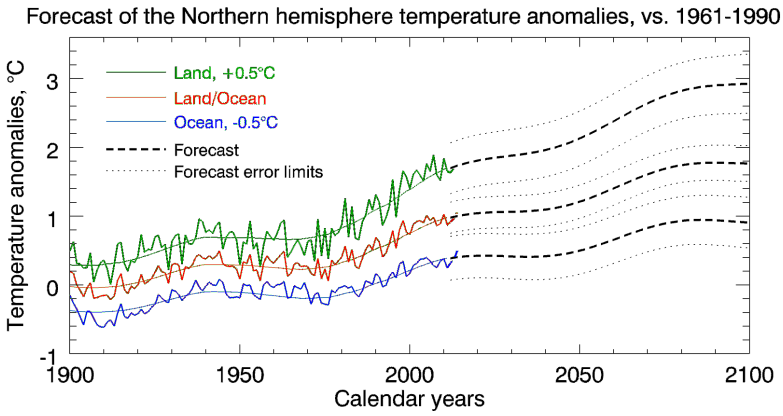

Fig.2. Observed global land, land/ocean and ocean NCDC temperature records and forecasts. The long term approximations are shown by thin continuous lines.

2.4. Temperature structural changes

The study of climate trends especially of the temperature trends taking into consideration possible structural changes is important for understanding the climate development itself and to find the correct answer whether the climate can be characterized by a stochastic trend or by a determined one. Here the global and hemisphere temperature anomalies are modeled by piecewise linear regression (see e.g. Green, 1993) to determine the break points in the temperature evolution, where a multitude of break point (BP) locations are simultaneously analyzed and the significances of slopes are tested. To choose the model the Schwarz-Bayesian Information Criterion (BIC) using the effective sample size (Seidel and Lazante, 2004) and the LWZ criterion (Liu et al., 1997) were used. The model with minimal criterion value was selected as the true model. In Fig.3 the studied here different observed global temperature time series and the resulting piece wise regression models for three BP's, where the LWZ criterion has minimal values are shown. To study the AMO influence on the structure changes from the temperature series the AMO influence was removed by subtracting the AMO temperature impact, obtained in the regression equations. The resulting temperature series were analysed by piecewise linear regression for structural changes. The results are shown in Fig.4.

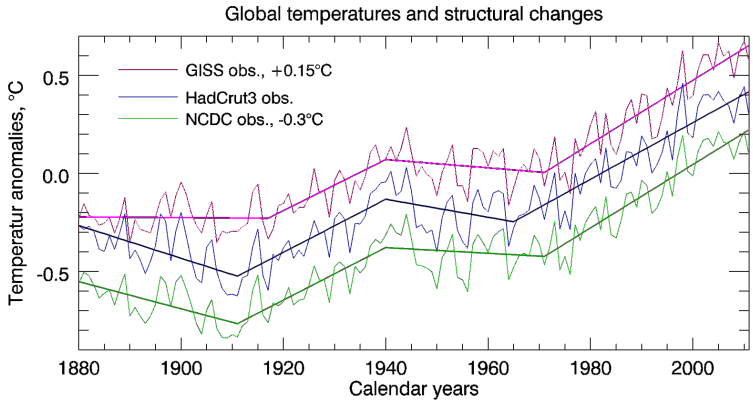

Fig.3. The global temperature anomalies by the three data sets. The thick lines show the structural models chosen by the LWZ criterion.

For the temperature series with removed AMO influences only one structural break point was found in every series. Hence, the break point structure for the original temperature series with three significant BP's is a result of the AMO temperature influence superimposed on the long time temperature evolution caused by CO_2. The single BP's in the AMO influence removed series corresponds to the third BP's found in the original temperature data, and they are shifted to earlier years, around 1960.

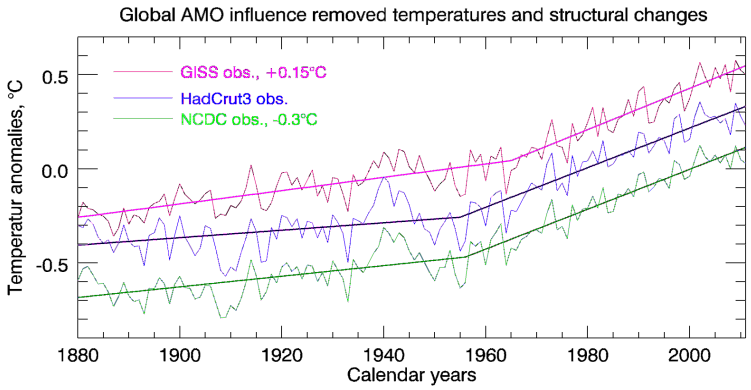

Fig.4. The same as in Fig 3 but for global temperature anomalies, where the AMO temperature influence was removed.

AMO influence on zonal temperatures

It was found that AMO has a strong influence only on the NH temperatures. To study the influences in more detail GISS zonal land temperatures were used, because of greater ocean temperature errors in the past. In Fig.5 the found dependences of the AMO temperature influence are presented. The AMO temperature influence increases from the Southern Subtropics to North. In the Antarctic zone and the Southern subtropic an anti-correlation to the zonal temperature is observed. The mean amplitude of the AMO index, used in the regressions, is about 0.2. The temperature influence of AMO on the Arctic temperature has a mean amplitude of 0.23°C, for example. The Latitude dependence of the AMO temperature influence is in accordance with the heat redistribution from South to North by an Artic Antarctic seesaw (Chylek et al., 2010).

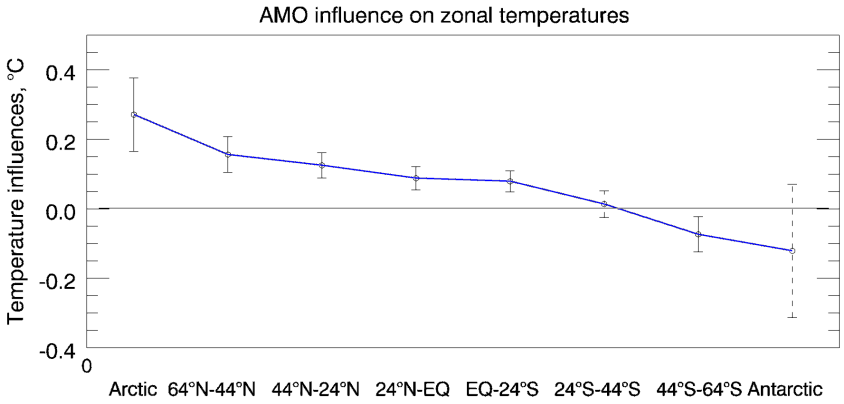

Fig.5. Latitude dependence of the AMO influence on the temperature, shown as dependences of the regression coefficients. For significant influences the error bars are presented by continuous line. In the case of non-significant influence the error bars passes and are drawn by dashed lines.

Conclusions

The found results demonstrated the important AMO influence on the temperature distribution and on the structural changes. The temperature oscillations generated by AMO have to be removed before the estimation of long time temperature trends.

References

The reference list of the cited in the text publications will be given on request.

Kinetics of electronically excited O2 molecules in the mixture of CO_2, CO, N_2, O_2 gases

Kirillov A.S. [1], *Werner R.* [2], *Guineva V.* [2]

[1] Polar Geophysical Institute of RAS, Apatity, Murmansk region, Russia
[2] Space Research and Technology Institute of BAS, Stara Zagora, Bulgaria
E-mail: rolwer52@yahoo.co.uk

Introduction

CO_2, CO, N_2, O_2 gases are the main components in the atmospheres of terrestrial planets. Electronically excited molecules play very important role in chemical kinetics of a mixture of atmospheric gases. It has been proposed by Toumi [1993], Siskind et al. [1993], Prasad [1997] that the interaction of $O_2(b^1\Sigma_g^+)$ with H_2 and N_2O molecules may significantly influence the chemistry of the stratosphere and upper troposphere of the Earth as a source of odd-hydrogen (HO_x) or odd-nitrogen (NO_x).

$O_2(b^1\Sigma_g^+)$ molecules are effectively produced in the atmosphere of the Earth at altitudes between 80 and 110 km. Three-body collisions

$$O + O + M \rightarrow O_2^* + M \qquad (1)$$

are main production mechanism of electronically excited molecular oxygen at the altitudes of the nightglow in the atmosphere of the Earth [Slanger and Copeland, 2003]. Spontaneous radiative transitions from the $b^1\Sigma_g^+$ state to the ground $X^3\Sigma_g^-$ state lead to emissions of Atmospheric bands in the nightglow of the atmosphere.

$$O_2(b^1\Sigma_g^+,v) \rightarrow O_2(X^3\Sigma_g^-,v') + h\nu_{Atm} \ . \qquad (2)$$

A study of excitation, quenching, and energy transfer processes in the oxygen nightglow on Venus and Mars by Krasnopolsky [2011] has considered altitude profiles of $[O_2(b^1\Sigma_g^+)]$ in atmospheres of the planets. The study was based on the observed nightglow intensities and vertical profiles, measured reaction rate coefficients, and photochemical models of the nighttime atmospheres of the Venus and Mars. Krasnopolsky [2011] has analysed mainly the kinetics of $O_2(b^1\Sigma_g^+,v=0)$, but detailed study of $O_2(b^1\Sigma_g^+,v\geq0)$ needs a set of the quenching constants for collisions with molecules of main gases in atmospheres of the planets.

The quenching rate coefficients

We apply the Rosen-Zener approximation to calculate the removal rates of O_2^* in inelastic collisions with CO_2, CO, N_2, O_2 molecules [Kirillov, 2004a,b]. The quenching rates of the $b^1\Sigma_g^+,v$=1-15 state by O_2 molecules are calculated with the consideration of intermolecular (EE-processes) transfers of electronic excitation [Kirillov, 2012]

$$O_2(b^1\Sigma_g^+,v) + O_2(X^3\Sigma_g^-,v=0) \rightarrow O_2(X^3\Sigma_g^-,v') + O_2(a^1\Delta_g,b^1\Sigma_g^+;v'') \ . \qquad (3)$$

Also we consider EV-processes of removal in the collisions with N_2, CO, CO_2, O_2 molecules

$$O_2(b^1\Sigma_g^+,v) + N_2(X^1\Sigma_g^+,v=0) \rightarrow O_2(a^1\Delta_g,v') + N_2(X^1\Sigma_g^+,v=1) \ , \qquad (4)$$

$$O_2(b^1\Sigma_g^+,v) + CO(X^1\Sigma^+,v=0) \rightarrow O_2(a^1\Delta_g,v') + CO(X^1\Sigma^+,v=1), \qquad (5)$$

$$O_2(b^1\Sigma_g^+,v) + CO_2(X^1\Sigma_g^+,0,0,0) \rightarrow O_2(a^1\Delta_g,v') + CO_2(X^1\Sigma_g^+,1,0,1) \ , \qquad (6)$$

$$O_2(b^1\Sigma_g^+,v) + O_2(X^3\Sigma_g^-,v=0) \rightarrow O_2(a^1\Delta_g,v') + O_2(X^3\Sigma_g^-,v=1). \qquad (7)$$

Here there are the transitions of electronically excited O_2^* molecules in another excited state with vibrational excitation of the ground state of target molecules. Moreover, we take into account the processes of VV-processes of energy exchange in the collisions with carbon dioxide molecules

$$O_2(b^1\Sigma_g^+,v) + CO_2(X^1\Sigma_g^+,0,0,0) \rightarrow O_2(b^1\Sigma_g^+,v\text{-}1) + CO_2(X^1\Sigma_g^+,1,0,0)\ . \qquad (8)$$

The process (8) means that the $O_2(b^1\Sigma_g^+,v)$ molecule losses one vibrational quantum of the $b^1\Sigma_g^+$ state and the energy transforms in vibrational quantum of symmetric stretch mode of CO_2 molecule.

The calculated quenching rate coefficients for the $b^1\Sigma_g^+,v$=1-15 state in the collisions (3-8) with O_2, N_2, CO, CO_2 molecules are presented in Fig.1. The calculations have shown that the quenching is very efficient in the collisions with O_2 molecules for high vibrational levels of this singlet state. More effective quenching by carbon dioxide molecules is seen for lower vibrational states of the $b^1\Sigma_g^+$ state.

The calculated quenching rate coefficients of electronically excited O_2 molecules are used in the simulations of vibrational populations of O_2 electronic states in the mixture of gases.

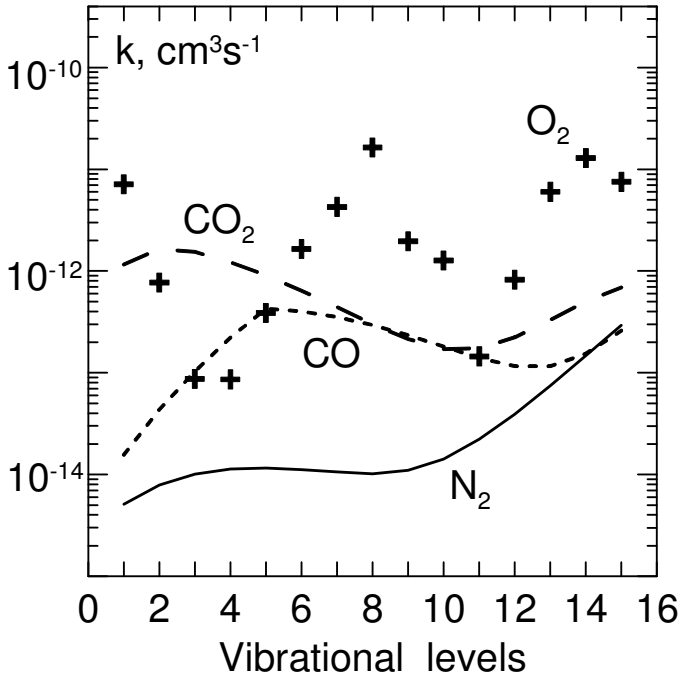

Fig.1. *The calculated quenching rate coefficients for the* $b^1\Sigma_g^+,v$=1-15 *state in the collisions with* O_2, N_2, CO, CO_2 *molecules (crosses; solid, short-dashed, long-dashed lines, respectively).*

Vibrational populations of O2(b1Σg+) in the mixture

It is suggested that three-body collisions (1) are the production mechanism of initially excited O_2. Vibrational populations of singlet oxygen are calculated at mixture pressures of 10^{-1}-10^0 Pa. The removal rates are taken according to the data presented in Fig.1.

The calculated vibrational populations of singlet $b^1\Sigma_g^+,v$=1-15 state of molecular oxygen in the mixture of O_2^* with the gases N_2, CO, CO_2 at pressures of 10^{-1}-10^0 Pa are shown in Fig.2. Also the experimental data of populations estimated from spectrometric observations from Keck-I telescope [Slanger et al., 2000] are presented in Fig.2. Slanger et al. [2000] have observed the intenities of Atmospheric bands (2) emitted from fifteen vibrational levels of the singlet state in the nightglow of the Earth.

It is seen from this figure that the behaviour of the populations in the cases of N_2-O_2 and CO-O_2 mixtures are similar. The principal influence of carbon dioxide molecules is seen in the case of CO_2-O_2 mixture. This mixture is an analogue of Venus and Mars atmosphere at the altitudes of the nightglow. It is seen from Fig.2 that there is an increase of relative populations of highest vibrational levels in comparison with ones of lowest levels. The difference in the behaviour of the populations for the mixtures can be explained by the removal rates presented in Fig.1.

The results of the calculations can be applied in the study of electronic kinetics of O_2^* at the altitudes of nightglows in the atmospheres of terrestrial planets and in active mediums of laboratory discharges and lasers.

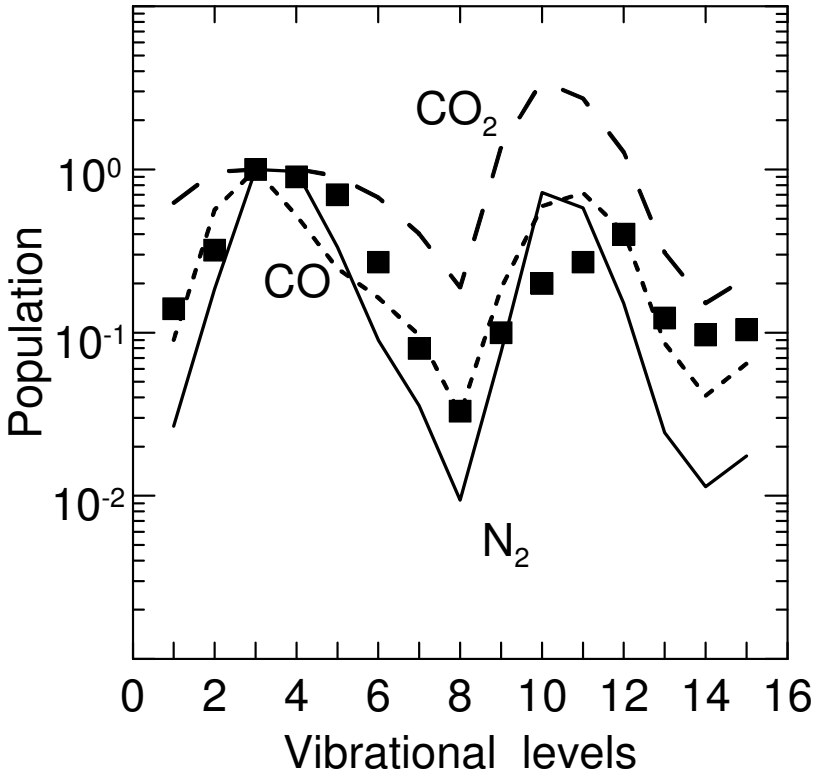

Fig.2. The calculated vibrational populations of singlet $b^1\Sigma_g^+$,v=1-15 state of molecular oxygen in the mixture of O_2^* with the gases N_2 (solid line), CO (short-dashed line), CO_2 (long-dashed line); experimental data by Slanger et al . [2000] – squares.

Conclusions

The main results of this presentation are as follows.

1. Applying the Rosen-Zener approximation we have calculated the removal rates of $O_2(b^1\Sigma_g^+,v)$ in inelastic collisions with CO_2, CO, N_2, O_2 molecules. The calculation has taken into account EE (3), EV (4-7) and VV (8) electron energy transfer processes.

2. Using the calculated removal rate constants we have simulated vibrational populations of singlet $b^1\Sigma_g^+$,v=1-15 state of molecular oxygen in the mixture of O_2^* with the gases N_2, CO, CO_2 at pressures of 10^{-1}-10^0 Pa. The results of the calculation show the principal dependence of the populations on the kind of admixture gas. The dependence can be explained by peculiarities of removal rates of $O_2(b^1\Sigma_g^+)$ in inelastic collisions with another molecules.

References

Kirillov A.S. Application of Landau-Zener and Rosen-Zener approximations to calculate rates of electron energy transfer processes. // Adv. Space Res., 2004a, v.33, p.993–997.

Kirillov A.S. Calculation of rate coefficients of electron energy transfer processes for molecular nitrogen and molecular oxygen. // Adv. Space Res., 2004b, v.33, p.998–1004.

Kirillov A.S. Calculation of rate coefficients for the interaction of singlet and triplet vibrationally excited oxygen. // Quantum Electronics, 2012, v.42, p.653-658.

Krasnopolsky V.A. Excitation of the oxygen nightglow on the terrestrial planets. // Planet. Space Sci., 2011, v.59, p.754-766.

Prasad S.S. Potential atmospheric sources and sinks of nitrous oxide. 2. Possibilities from excited O_2, "embryonic" O_3, and optically pumped excited O_3. // J. Geophys. Res., 1997, v.102, p.21527-21536.

Siskind D.E., Summers M.E., Mlynczak M.G. An evaluation of $O_2(b^1\Sigma_g)$ as a possible source of OH and odd-nitrogen in the stratosphere and mesosphere. // Geophys. Res. Lett., 1993, v.20, p.2047-2050.

Slanger T.G. and Copeland R.A. Energetic oxygen in the upper atmosphere and the laboratory. // Chem. Rev., 2003, v.103, p.4731-4766.

Slanger T.G., Cosby P.C., Huestis D.L., Osterbrock D.E. Vibrational level distribution of $O_2(b^1\Sigma_g^+,v=0\text{-}15)$ in the mesosphere and lower thermosphere region. // J. Geophys. Res., 2000, v.105, p.20557-20564.

Toumi R. A potential new source of OH and odd-nitrogen in the atmosphere. // Geophys. Res. Lett., 1993, v.20, p.25-28.